Numerical Weather Prediction

Improving Tropical Performance.
I - Diagnosing errors in the New Unified Model (cycle G27)

Forecasting Research Technical Report No. 401

Sean Milton, Ian Culverwell, Glenn Greed and Martin Willett

email: nwp_publications@metoffice.com

Forecasting Research Technical Report No. 401

Improving Tropical Performance:
I - Diagnosing errors in the New Unified Model (cycle G27).

Sean Milton, Ian Culverwell, Glenn Greed, and Martin Willett

12 February 2003

1. Introduction

In August 2002 the Met Office implemented a new Unified Model (global model cycle G27 - see appendix) which consisted of a reformulation of the dynamical core ("New Dynamics") and the introduction of a new physics package. An outstanding issue at the time of the operational implementation was the degradation in some aspects of tropical performance compared to the old operational model (cycle G26). These included deterioration of the wind verification scores, increased tropical circulation errors, and a tendency to produce gridpoint storms (GPS). On the positive side, and perhaps surprisingly, there were marked improvements in the prediction of tropical cyclones (Heming and Greed, 2002). Despite the tropical degradations, cycle G27 was implemented operationally on the 7th August 2002 on the strength of performance gains in the extratropics.

This paper presents diagnostics from the trial forecasts of the new Unified Model in an attempt to understand possible reasons for degraded tropical performance. This forms the starting point for the follow on project in 2002/03, FC03FR "Improving tropical performance", and for a similar team investigating poor tropical performance in the next coupled climate version of the Unified Model (HadGEM1).

2. Model Experiments

The diagnostics shown in this paper are largely derived from experiments run over the four seasons at full operational resolution (N216) with data assimilation (see table below). The control was the Unified Model version in use operationally prior to 7th August 2002. The Mar-Apr 2001, Sep-Oct 2001 and Jan-Feb 2002 controls all included data assimilation upgrades made operational during autumn 2001 (cycle G26 - see appendix for details). The control for the Jun-Jul 2001 season was global model cycle G25 operational at that time. The experiments were with a development version 4.7 of cycle G27, which in all important respects was the same as the final version implemented. The assimilation in the experiments was set up to match the controls, with Mar-Apr 2001, Sep-Oct 2001, and Jan-Feb 2002 including the autumn 2001 assimilation upgrades.

	Jan-Feb 2002[1]	Mar-Apr 2001	Jun-Jul 2001	Sep-Oct 2001
Start	11 Jan 2002	10.03.2001	21.06.2001	20.09.2001
End	25 Feb 2002	07.04.2001	20.07.2001	18.10.2001

Results from a large number of N144 resolution experiments are also used to illustrate sensitivity of the model's tropical performance to certain changes in formulation.

3. New Unified Model Formulation - Cycle G27

The New Dynamics is outlined in Cullen et. al. (1997) and described in detail in Staniforth et. al (2002). The numerics consist of a two time-level semi-implicit, semi-lagrangian scheme replacing a split-explicit time integration and Eulerian advection (Cullen and Davies, 1991). The vertical coordinate is terrain following hybrid height utilising the Charney-Phillips grid staggering in the vertical in place of the Lorenz grid and a pressure based vertical coordinate. The New Dynamics has a non-hydrostatic formulation, even for the synoptic scale predictions of the global model. In the horizontal, the Arakawa C grid staggering replaces the B grid

[1] The period for the objective verification was different to that for the diagnostics being 19.12.2001 to 24.01.2002.

staggering. The New Dynamics is typically run with less explicit diffusion than the old operational model. The vertical resolution of the new model has been increased from 30 to 38 levels, with all of the additional levels being placed in the boundary layer.

In addition to the improvements to the dynamical core of the model, a large number of improvements to the physical parametrizations have also been introduced (loosely based on the HadAM4 physics package developed for the climate version of the Unified Model). These include a revised radiation scheme (Edwards and Slingo, 1996), a mixed phase microphysics (Wilson and Ballard, 1999), a new turbulent boundary layer scheme (Lock et. al., 2000), improvements to convection-BL interaction (Version 4A convection scheme - see discussion below), a representation of the radiative effect of convective anvils (Gregory, 1999), a revised cloud area parametrization which allows cloud to fill only part of the thickness of a vertical layer (vertical cloud gradient - S.Cusack (pers. comm.)), a new orographic gravity wave drag (GWD) parametrization and new GLOBE orography dataset (smoothed with Raymond filter) (Webster et. al., 2002).

The list below highlights a number changes which impacted directly on tropical performance. These were part of the version used for the full resolution data assimilation trials.

- Version 4A convection (originally referred to as CMODS6)[2]
  - *Diagnosis of deep and shallow convection*. Based upon parcel ascent as for the boundary layer type diagnosis adopted in the new boundary layer scheme.
  - *Convective cloud base is defined at the LCL*. The boundary layer scheme is prevented from operating above this, so no longer overlaps with convection.
  - *New parametrization for convective momentum transports* now based on a flux-gradient relationship. This is obtained from the stress budget by parametrizing the terms (by analogy with scalar flux budgets) such that there is a gradient term associated with the mean wind shear (involving an eddy viscosity) and a non-gradient term associated with the transport (using a mass flux approximation).
  - *New cloud-base closures for thermodynamics and momentum transport*. The thermodynamic closure for shallow convection relates the cloud-base mass flux to a convective velocity scale (Grant and Brown, 1999). For deep convection, the thermodynamic closure is based on the reduction to zero of convective available potential energy (CAPE) over a given timescale (based on Fritsch and Chappell, 1980). The momentum transport closure for deep and shallow convection is based on the assumption that large-scale horizontal pressure gradients should be continuous across cloud base.
  - *parametrized entrainment and detrainment rates for shallow convection* are obtained using similarity theory by assuming that the entrainment rate is related to the rate of production of TKE (Grant and Brown, 1999). Entrainment rates are larger for shallow convection than deep, reflecting observational evidence (Esbensen, 1978) and large eddy simulations (Siebesma and Cuijpers, 1995).
- Vertical diffusion in the tropics - this was introduced to improve 250hPa wind scores. The old operational version (cycle G26 and earlier) has always used vertical diffusion in the tropics (see section 7.4).
- Moisture diffusion - originally only diffusion of winds and potential temperatures was carried out, but diffusion of moisture was found to be beneficial in controlling gridpoint storms.

[2] Personal communication from Alan Grant and Gill Martin.

- Relative humidity (RH) based CAPE closure - CAPE closure varies from 1 hour to a few minutes as a linear function of RH between 70% and 100%. This is intended to help alleviate grid point storms by removing instability in the column over a short timescale. In the model the CAPE closure operates at close to 1 hour in most situations, which was the timescale used in cycle G26.

4. Objective Verification

We begin by considering the performance of the new Unified Model in the tropics in terms of objective verification measures from the N216 trials. For the remainder of this paper we shall use the global model cycles to reference the experiments and controls as follows[3]

- **Cycle G26** - control - operational model prior to 7th August 2002.
- **Cycle G27** - experiment - New Dynamics and revised physics.

4.1. Error growth in 850hPa and 250hPa tropical winds.

Figures 1-4 show the RMS vector wind errors (RMSVWE) for tropical winds at 250hPa and 850hPa. For verification against sondes at 250hPa G27 forecasts have consistently higher RMSVWE in all seasons and forecast ranges (Fig. 1). At 850hPa the G27 forecasts are better/neutral in Dec-Jan and Mar-Apr, but for Jun-Jul show increased error growth compared to G26 beyond T+24 (Fig. 2).

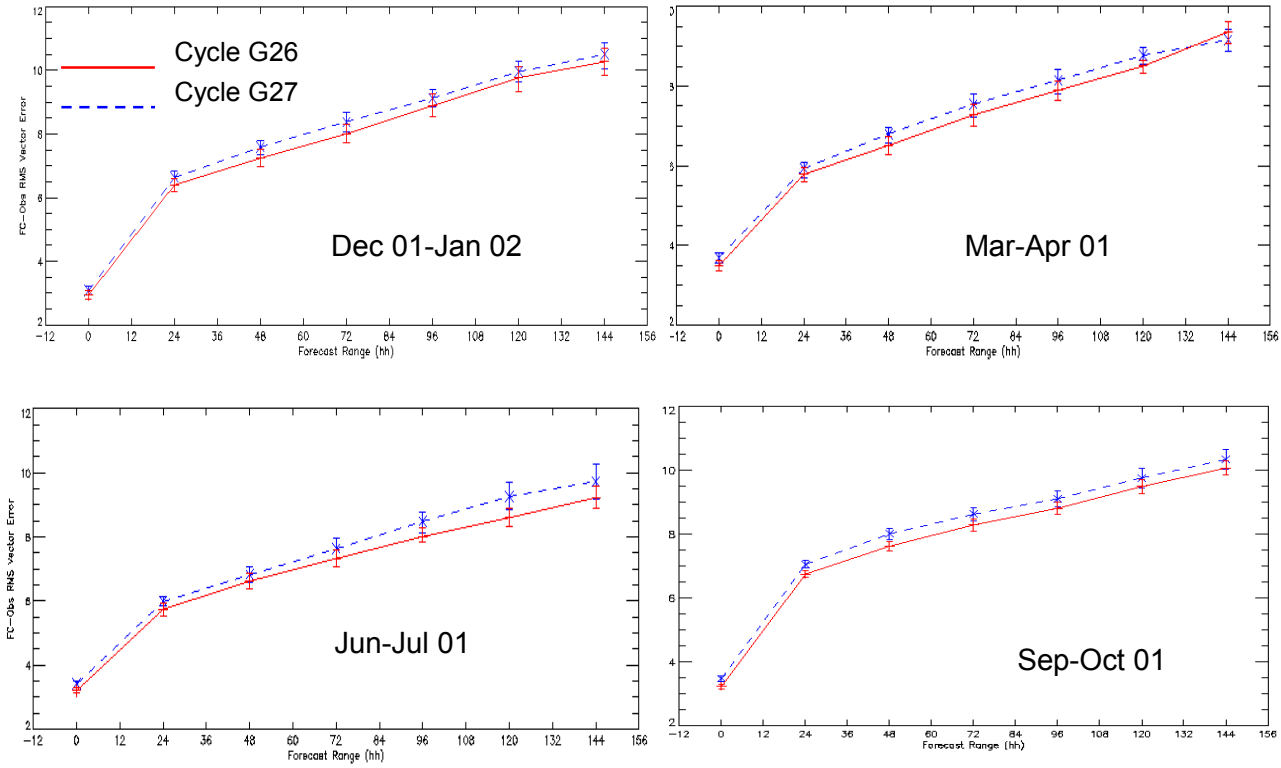

Figure 1:*RMS vector wind errors for 250hPa winds over tropical domain (20N-20S) for N216 trials over four seasons in 2001-2002. Verification is against sondes. Units - m/s*

[3] Note - the figures often use OP or vn4.5 to refer to the controls (cycle G26) and ND, NDHadAM4, or vn5.2 to refer to the new Unified model (cycle G27). The figure captions will use the naming convection of G26 and G27 to be consistent with the discussion in the main text.

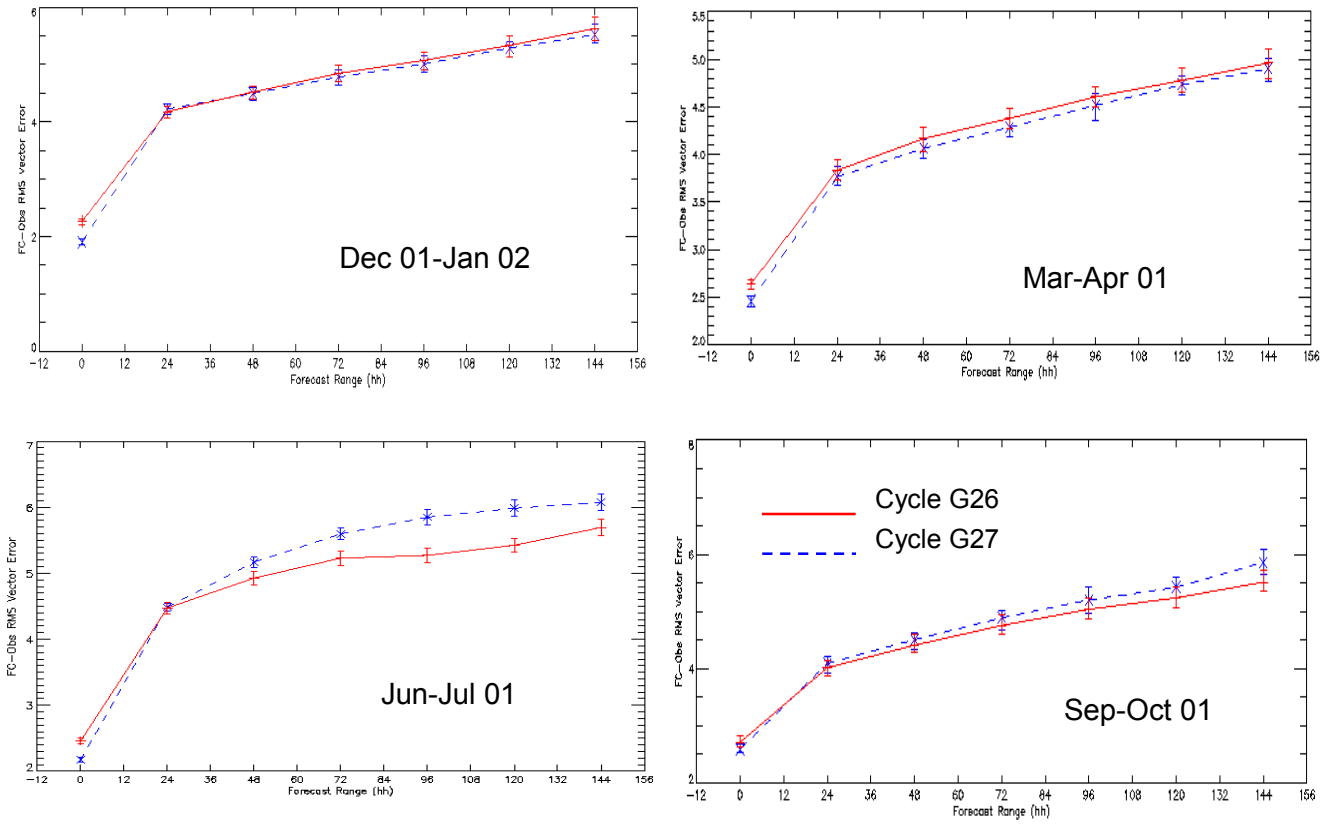

Figure 2 *- as figure 1 but for 850hPa winds. Verification vs. sondes.*

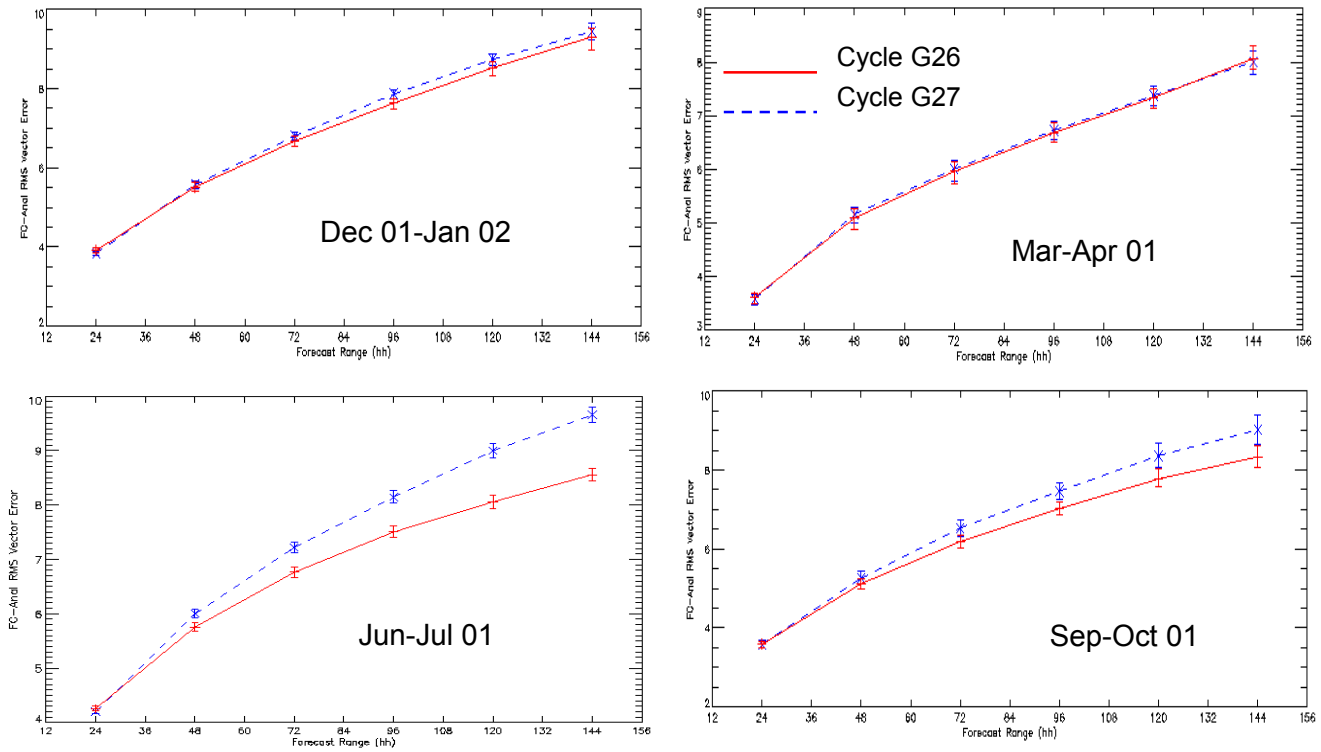

Figure 3:*RMS vector wind errors for 250hPa winds over tropical domain (20N-20S) for N216 trials over four seasons in 2001-2002. Verification is against analyses. Units - m/s*

RMSVWE's are also increased in Sep-Oct but not as much as in Jun-Jul. It is interesting that in all seasons the T+0 RMSVWE's at 850hPa are consistently less in G27 (Fig.2). This may reflect how closely the observations are fitted in G27 compared to G26. For verification against analyses the G27 250hPa winds show increased errors at T+48 and beyond in Jun-Jul and Sep-Oct, with smaller degradations in Dec-Jan and similar performance to G26 in Mar-Apr (Fig.3). At T+24 the errors in G27 and G26 are comparable in all seasons. Finally, at 850hPa we see similar signals to those seen for verification against sondes, with G27 worse in Jun-Jul and Sep-Oct and improved in Dec-Jan and Mar-Apr (Fig. 4).

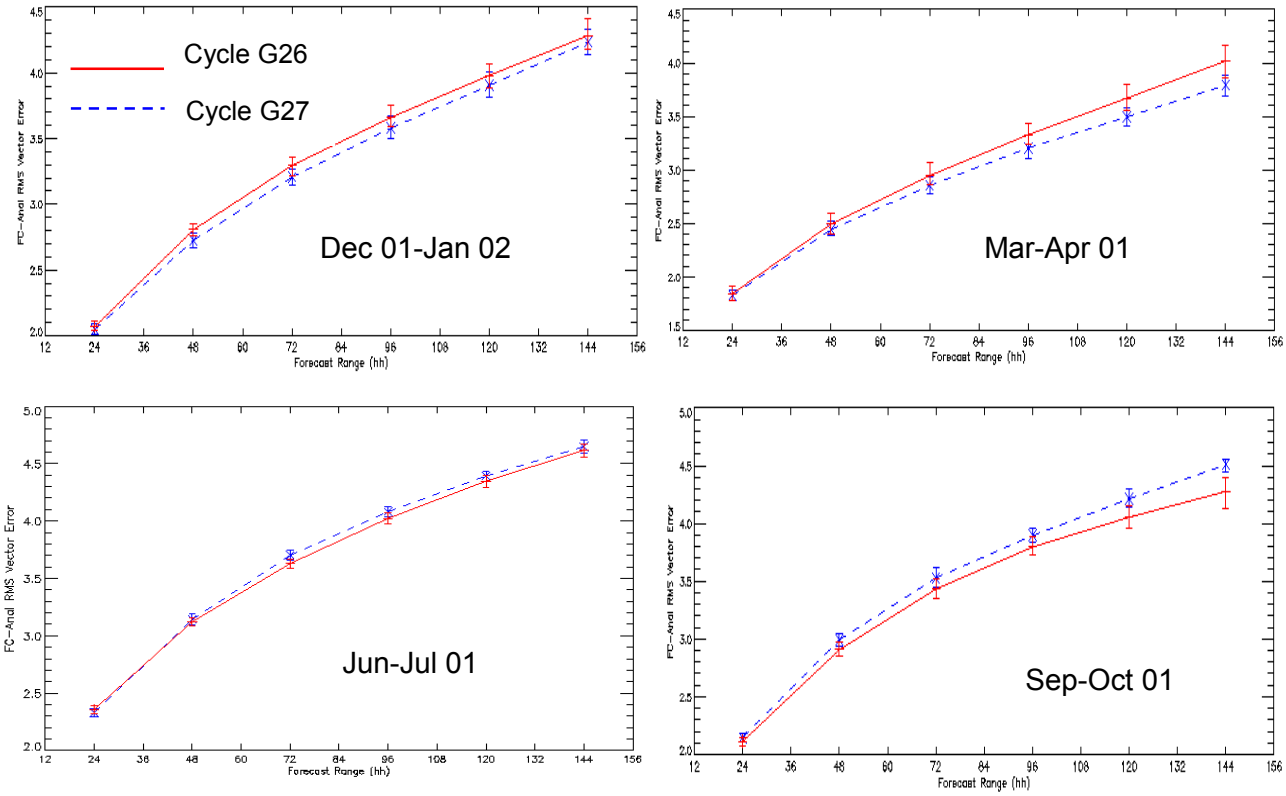

Figure 4 *- as figure 3 but for 850hPa winds. Verification vs. analyses.*

In summary, the biggest discrepancies in tropical performance between G27 and G26 appear to be in the Jun-Jul season.

4.2. Vertical variations in skill.

Obviously we have to be careful in interpreting tropical performance over only two tropospheric levels. Figure 5 shows the variation in T+72 RMSVWE's for Jun-Jul 2001 as a function of height (pressure). The largest errors in G27 do occur in the lower and upper troposphere. At 200hPa errors are ~12% larger than G26 for verification against analyses, although the peak errors occur at 150hPa. In the lower troposphere (1000-400 hPa) the G27 performance is more neutral against G26 for verification against analyses, but for verification vs. sondes the errors in G27 are ~14% larger than G26.

4.3. Geographical distribution of RMS Errors

For verification against analyses we can plot the geographical distribution of RMS errors, formed from the time series of forecast and analysis data at each grid point (i.e. over the number of cases in a trial). Figure 6 shows this diagnostic for T+24 250 hPa zonal wind (U)

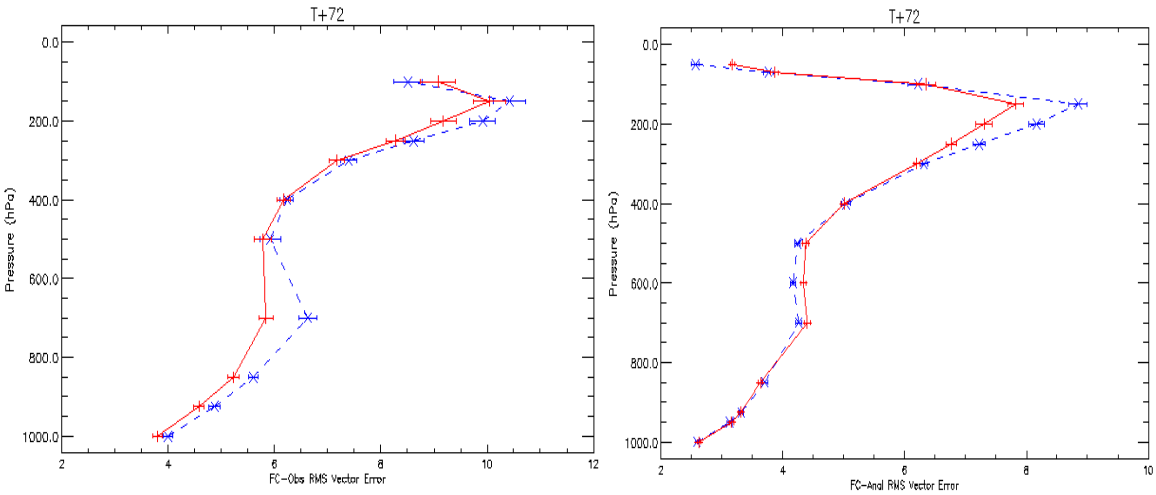

Figure 5 : T+72 RMS vector wind error over the tropical domain (20N-20S) as a function of height (pressure), for verification against sondes (left) and analyses (right). Results from Jun-Jul 01 trial period

forecasts during Jun-Jul 2001. Both models have similar RMS errors with largest errors located over the Indian Monsoon region. The difference plot for the RMS errors (Fig. 6 (bottom panel)) shows that over the whole tropical domain there are as many areas of reduced RMS errors as increased RMS errors for G27. This agrees with the error growth curves in figure 3, where at T+24 the G27 and G26 forecasts have similar errors. However, the larger errors in G27 tend to be located close to the equator.

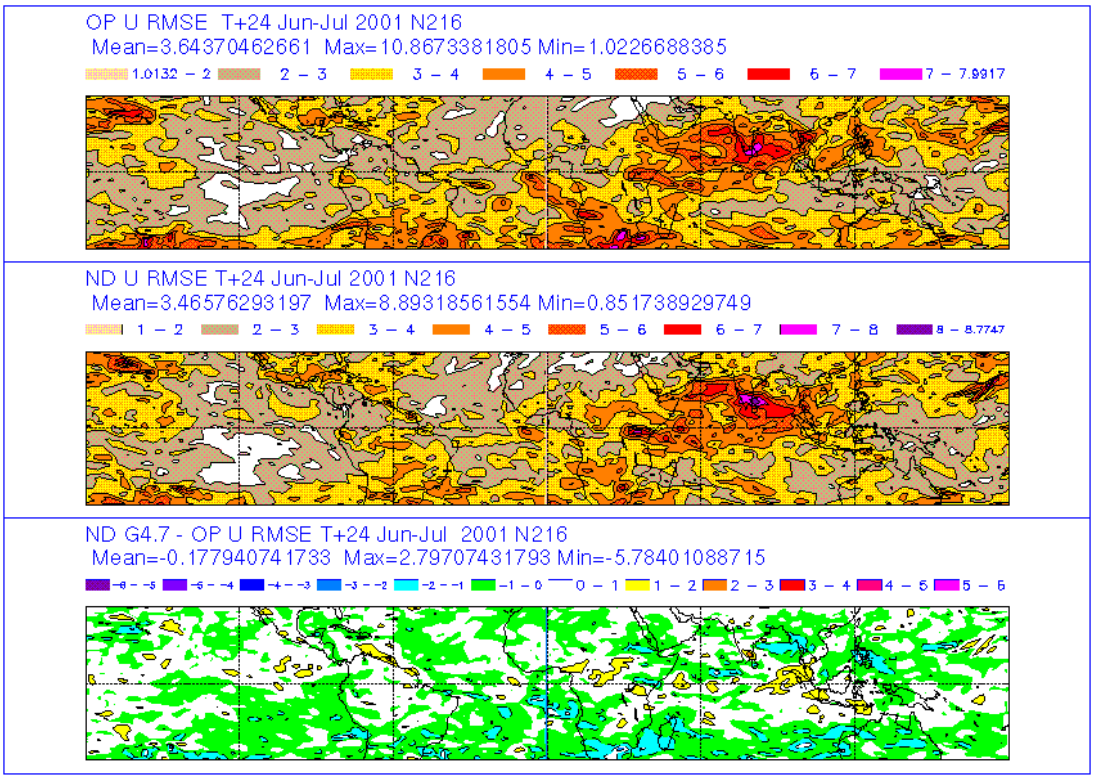

Figure 6: Spatial distribution of T+24 RMS errors for 250hPa zonal wind (U) showing G26 (top), G27 (middle), and G27-G26 (bottom). Results from Jun-Jul 2001 N216 trials. (See text for explanation of RMS error diagnostic).

At T+120 there is a clear signal of larger RMS errors in the G27 forecasts (Fig.7). The increased RMS errors are located in 3 main regions close to the equator, the east Pacific, the Atlantic, and Indonesia. These errors are generally equatorward of the areas of observed maximum precipitation (Fig. 8), shown by the global precipitation climatology project (GPCP - Huffman et. al, 1997) combined precipitation product (infrared estimate and raingauge) for June, July, and August 2001. In addition, we have areas of increased RMS error at around 25N in the East Pacific and subtropical Atlantic. It is also worth noting that the RMS error differences (Fig.7 bottom

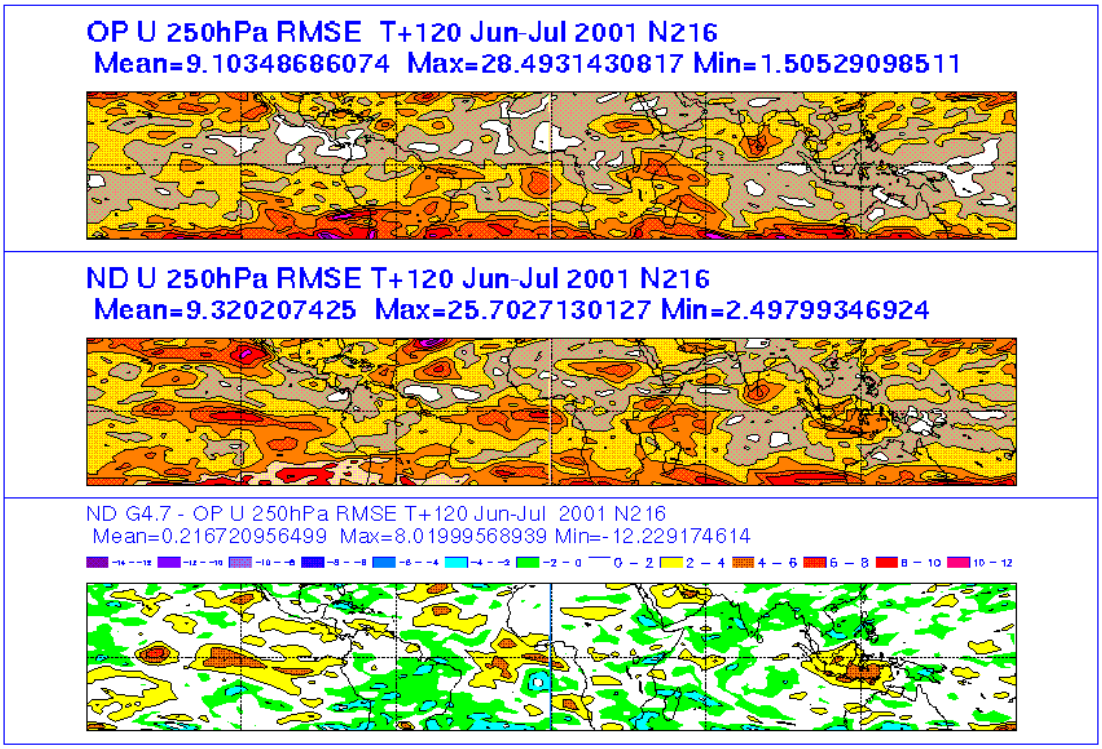

Figure 7: As Fig. 6 but for T+120 zonal wind forecasts. Contours/colours as in Fig. 6.

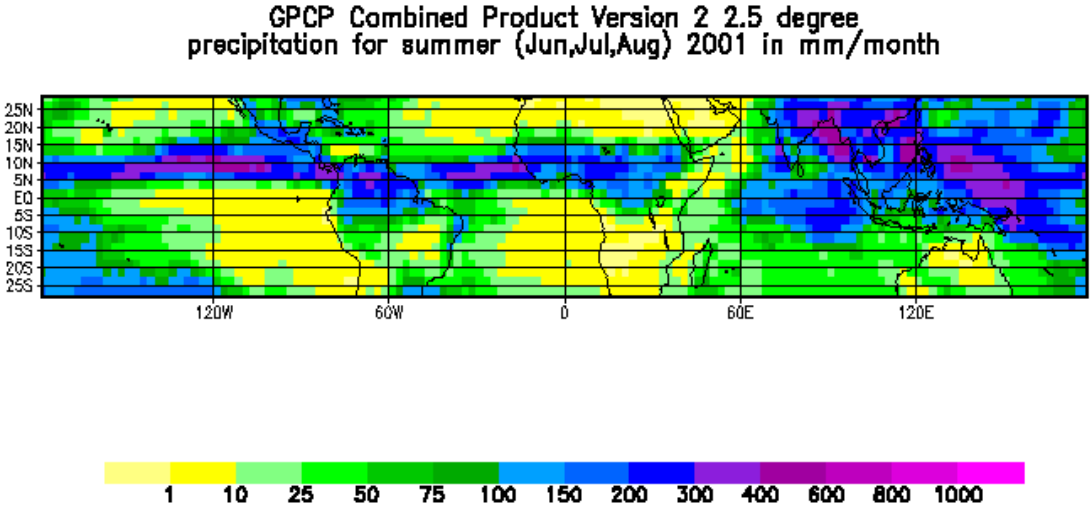

Figure 8: *GPCP combined precipitation product (gauge + IR) showing seasonal mean (mm/month) for JJA 2001.*

panel) are organised on large scales and are not just a function of increased "noise" in the G27 forecasts. This suggests the increased errors may be directly linked to errors in the forced tropical circulation.

4.4. Mean errors in 250hPa tropical winds

We can determine what contribution the mean errors make to the overall RMS errors by decomposing the mean square error into its random (primed quantity) and systematic component.

$$\overline{\varepsilon^2} = \overline{\varepsilon'^2} + \overline{\varepsilon}^2 \qquad \text{Equation 1}$$

Where, $\varepsilon = f - a$. The time mean errors in 250 hPa zonal wind show increased westerly flow in the same 3 equatorial locations where the RMS errors are increased (Fig.9). Figure 10 shows both the random RMS error and the total RMS error. Although the mean error does contribute to the total RMS error in these equatorial regions, there is still a contribution to the total error from the random/transient component. Elsewhere the mean error accounts for virtually all of the total RMS error. An example is the reduction in the upper tropospheric easterly jet in both G26 and G27 over the Sahara, Arabian Sea and India (Fig. 9 and 10).

4.5. Variability in tropical winds.

A further decomposition of the mean square error shows that the random component itself is made up of additional terms involving the forecast and the analysed variance (first 2 terms on RHS of eq. 2) and a third term which represents the covariance of forecast and analysed fields (represented in this equation by a correlation coefficient (R) - see Murphy (1988) for the derivation).

$$\overline{\varepsilon^2} = \sigma_f^2 + \sigma_a^2 + \overline{\varepsilon}^2 - 2.\sigma_f \sigma_a R \qquad \text{Equation 2}$$

Given a significant component of the RMS error in 250hPa tropical winds comes from the random error, it is useful to compare the terms in this equation. Figure 11 shows zonally averaged verification statistics for the 250hPa zonal wind field for the tropics during Dec-Jan and Jun-Jul. The RMS errors at T+120 (top panels - fig.11) reinforce points already discussed, namely that performance is worse in Jun-Jul and is particularly poor close to the equator. The T+24 RMS error is more comparable in G27 and G26.

The variance of the forecasts (middle panels - fig. 11) shows that in general both models have similar variance at a given forecast range. However, both show a clear systematic decrease in variance between T+24 and T+120 for both seasons. The one exception to this decreasing variance is in Jun-Jul. The T+120 variance in the G27 forecasts is much higher than its G26 counterpart in the equatorial region. From equation 2 we note that when all predictability is lost (R=0) and assuming there is no bias then the MSE will asymptote to

$$\overline{\varepsilon^2}_{Asymptote} = \sigma_f^2 + \sigma_a^2 \qquad \text{Equation 3}$$

If the forecast variance is underestimated in one model but not in the other then from eq. 3 the RMS errors in the approach to asymptotic limit will be trivially reduced in the forecast with reduced forecast variance.

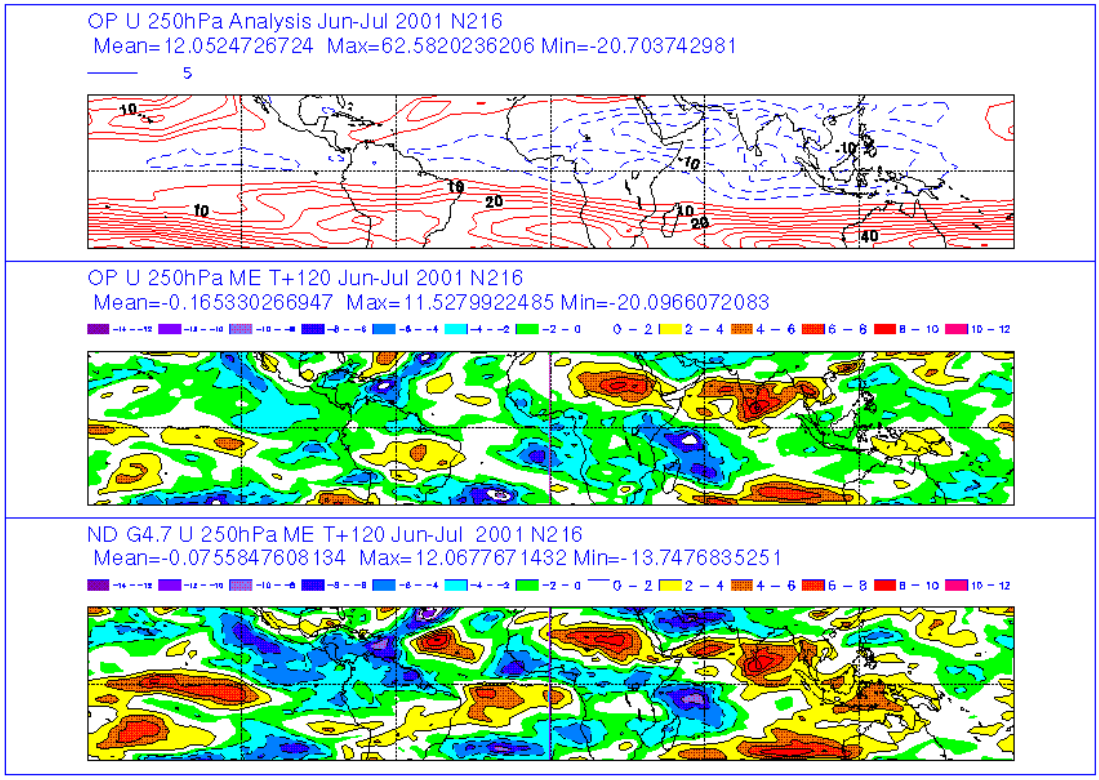

Figure 9: *250hPa zonal wind mean errors for T+120 forecasts. G26 analysis (top), G26 mean error (middle), and G27 mean error (bottom). For Jun-Jul 2001 trial.*

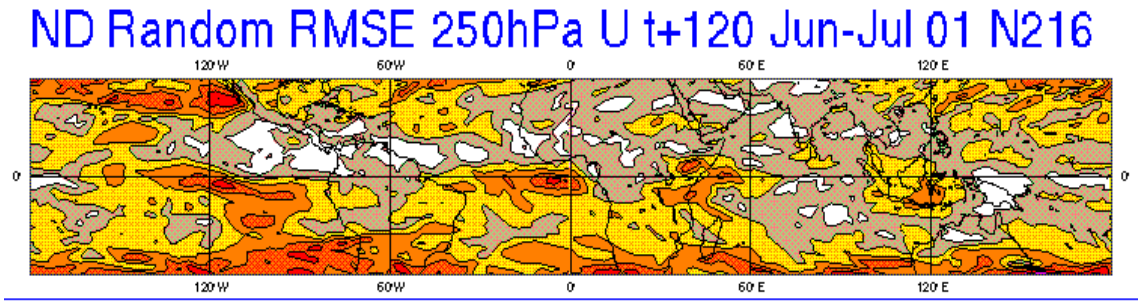

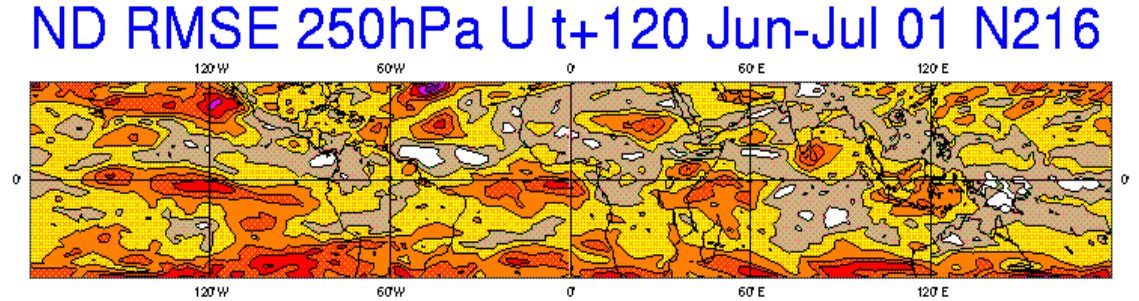

Figure 10: *Spatial distribution of T+120 RMS errors for 250hPa zonal wind (U) showing random RMS error (top), total RMS error (bottom). Results from Jun-Jul 2001 N216 trials. (See text for explanation of random RMS error diagnostic). Results are for cycle G27 forecasts.*

We can form a normalised mean square error (and RMS error) by dividing the MSE by the sum of the forecast and analysed variance (i.e. RHS of eq 3). This normalised RMSE ensures that in the asymptotic limit of error growth we don't favour a model version with a low level of variance relative to other versions or observations. This measure is directly related to the correlation coefficient (see Simmons et. al. (1995) for discussion). The normalised RMSE is shown in the bottom panels of figure 11. For Jun-Jul we see that after normalising by the variances, the equatorial region is still less skilful in G27. So the degraded performance in this region cannot be trivially explained as an artefact of increased variance in G27 forecast relative to G26. However, the variance field does play some role in modulating the RMS errors

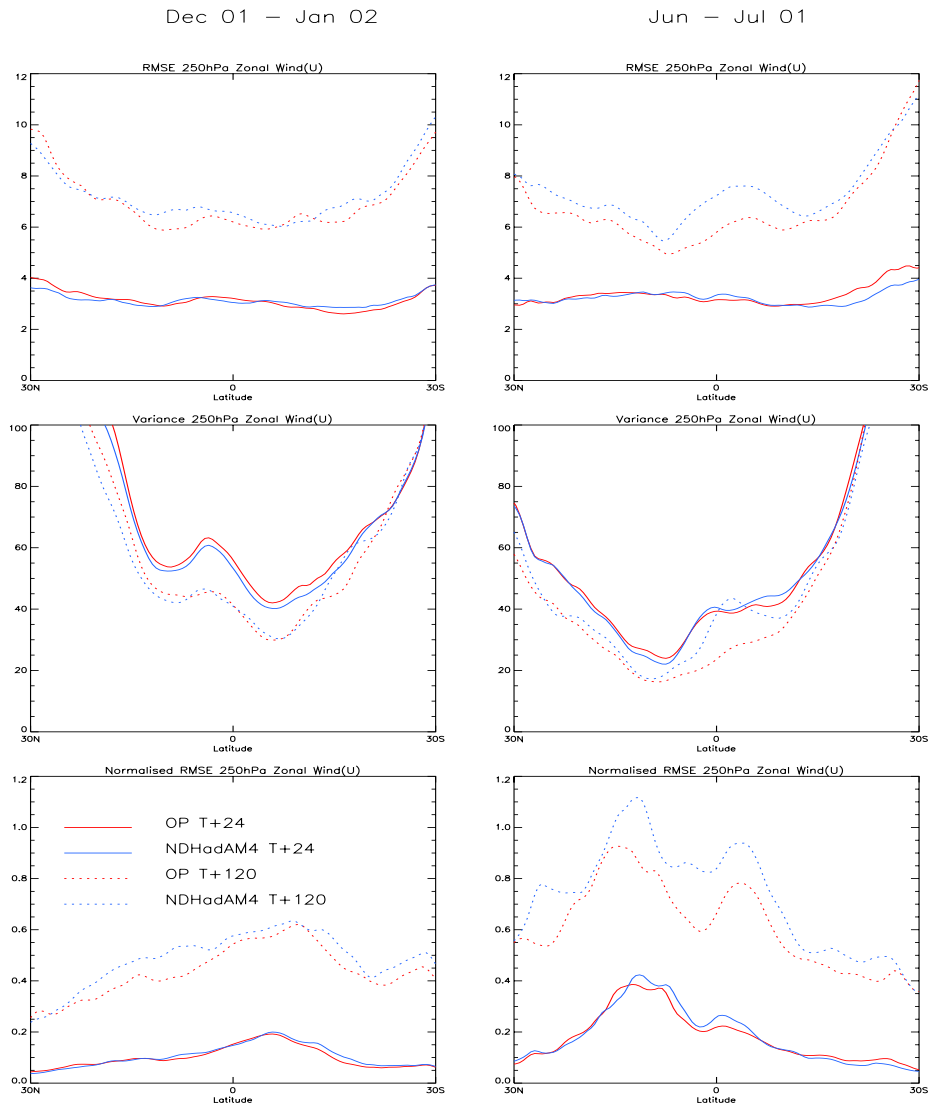

Figure 11 *- Zonally averaged verification statistics for 250hPa zonal wind. RMS error (top), Variance (middle), and normalised RMS error (bottom - see text for explanation). Cycle G26 (red) and cycle G27 (blue).*

as there is an even degradation in performance across the whole of the tropics at T+120 in G27 compared to G26, with the equatorial region no longer standing out as being worse than any other region. The Jun-Jul period is also less predictable than the Dec-Jan period, as seen by the normalised MSE being closer to its saturation value of one[4]. Further work on evaluating

[4] The normalized RMS error exceeds 1 in some places because we have not removed the mean error contribution (see equation 2).

tropical variability in the Unified Model may shed more light on model errors. Wavenumber-frequency diagnostics such as those used by Wheeler and Kiladis (1999) to examine convectively coupled equatorial waves could be very useful in this respect.

5. Tropical Circulation - winds

In this section we look in more detail at the time-mean tropical circulation and in particular at systematic errors in the rotational and divergent components of the circulation.

5.1. Hadley Circulation

The zonally averaged meridional wind (Fig.12) and the meridional wind errors and analysis/forecast differences (Fig.13) show that there is a marked increase in the strength of the Hadley circulation in the G27 forecasts by T+120. The error field shows too strong a flow southwards at 250hPa, which increases the meridional wind at this location by ~1 m/s. There appears to be a compensating return flow (northward) in the mid-troposphere. In the lower troposphere there is a negative error (winds too southerly), which implies a tendency to damp the northward flow in the boundary layer. This three cell structure in the meridional wind error is interesting. It may be linked to errors in the vertical distribution of parametrized diabatic heating in the model. The errors in the G26 forecasts are structurally very similar, but are only half the magnitude of those in the G27 forecasts. For Dec-Jan there is also an increase in the Hadley circulation in G27 forecasts (not shown), but the errors are not as large as in the Jun-Jul season.

5.2. Divergent flow errors in Jun-Jul forecasts - velocity potential

We can use the velocity potential to examine the geographical distribution of the planetary scale errors in the divergent flow. For Jun-Jul the analysed 250hPa velocity potential shows divergence (implied ascent) over the SE Asian sector and convergence (implied descent) in the subtropical Atlantic and east Pacific (Fig. 14). Both models have similar errors in velocity potential, with increased divergence in the Indian Ocean and increased convergence in the east Pacific. However, the error in the G27 forecasts is typically twice as large as G26. At 850hPa we see the reverse errors to 250hPa, with increased convergence over the Indian Ocean and increased divergence over the east Pacific (not shown). The errors in divergent flow for the Jan-Feb forecasts are similar to those from the Jun-Jul forecasts, but the differences between G26 and G27 are less extreme. These errors in 250hPa and 850hPa velocity potential imply an increase in the east-west Walker circulation over the Pacific.

5.3. Rotational flow errors in Jun-Jul forecasts - streamfunction

One possible reason for increased convergence/divergence at 850/250hPa in the Indian Ocean could be increased diabatic heating in this region. The dominant balance in the tropics is between vertical motion and heating. Consequently errors in heating quickly project onto errors in the vertical motion field and the divergent circulation. The linear analytical model of tropical flow due to Gill (1980) and Matsuno (1966) predicts the likely rotational errors to be an anomalous Kelvin wave to the east of the anomalous/erroneous heat source with increased low level easterly flow and increased upper level westerly flow. To the west of an erroneous heat source the Gill-Matsuno model predicts a Rossby wave response in the error field with twin cyclonic errors in the lower troposphere and anticyclonic errors in the upper troposphere. Considering the 850hPa streamfunction we do see some of the features discussed above (Fig. 15). Both G27 and G26 have increased easterly flow along the equator, with the easterlies in the G27 being more intense than in G26, consistent with the larger divergent flow errors (Fig.14). Examination of a time sequence of wind errors shows that the easterly errors over the

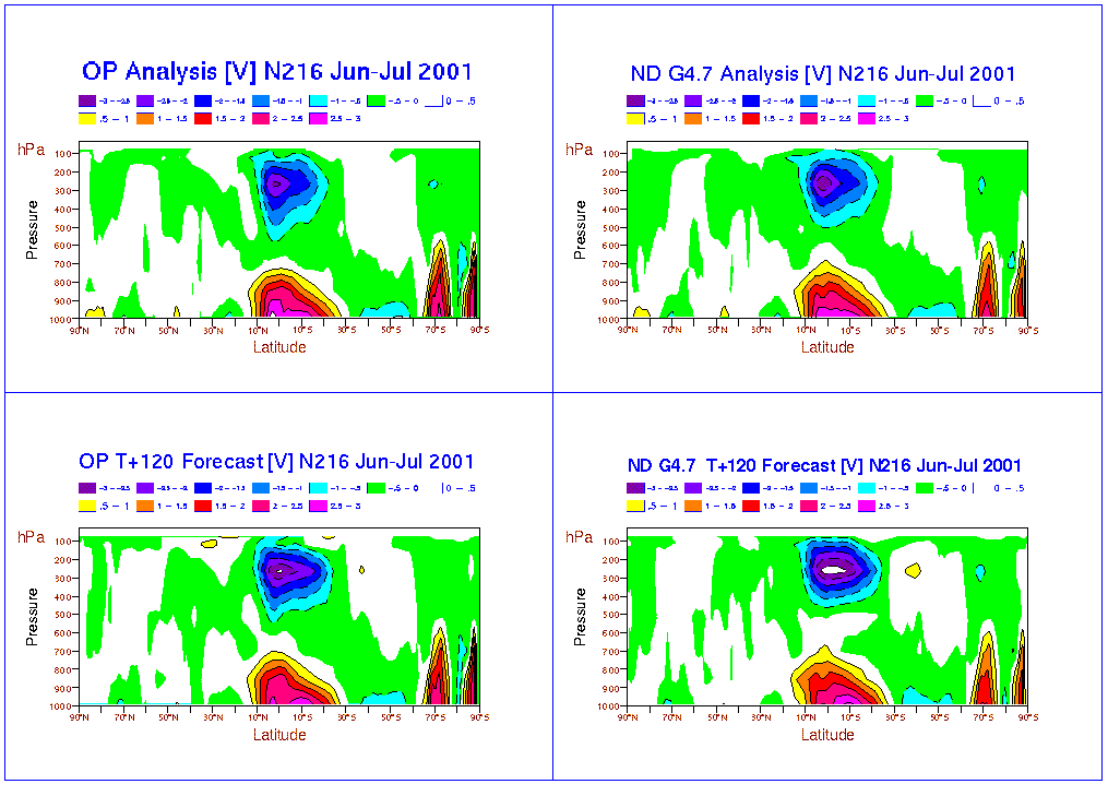

Figure 12 *- Hadley circulation for G27 and G26 analyses and T+120 forecasts for Jun-Jul 2001. Contour interval is 0.5 m/s*

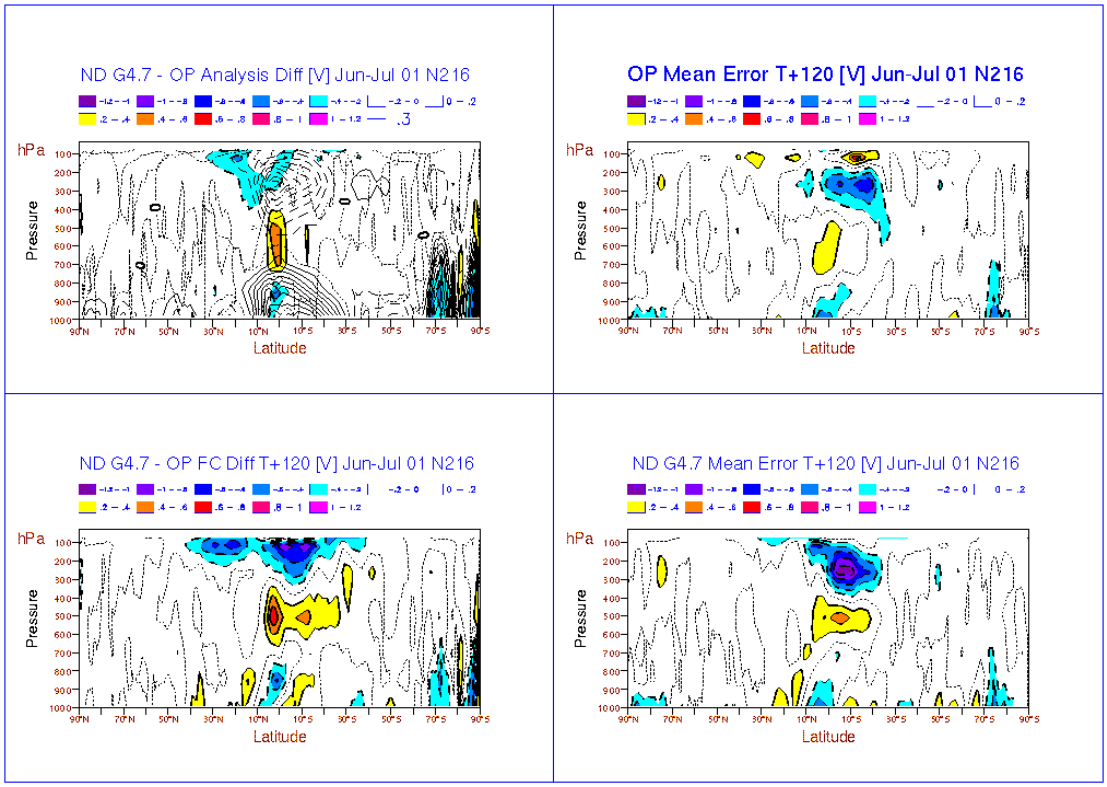

Figure 13: *Hadley circulation for G27 and G26. Showing analysis (G27) and analysis difference (G27 - G26) (top right), G26 T+120 forecast mean error (top right), forecast difference (G27 - G26) (bottom left), G27 T+120 forecast mean error (bottom right). Contour interval is 0.2 m/s.*

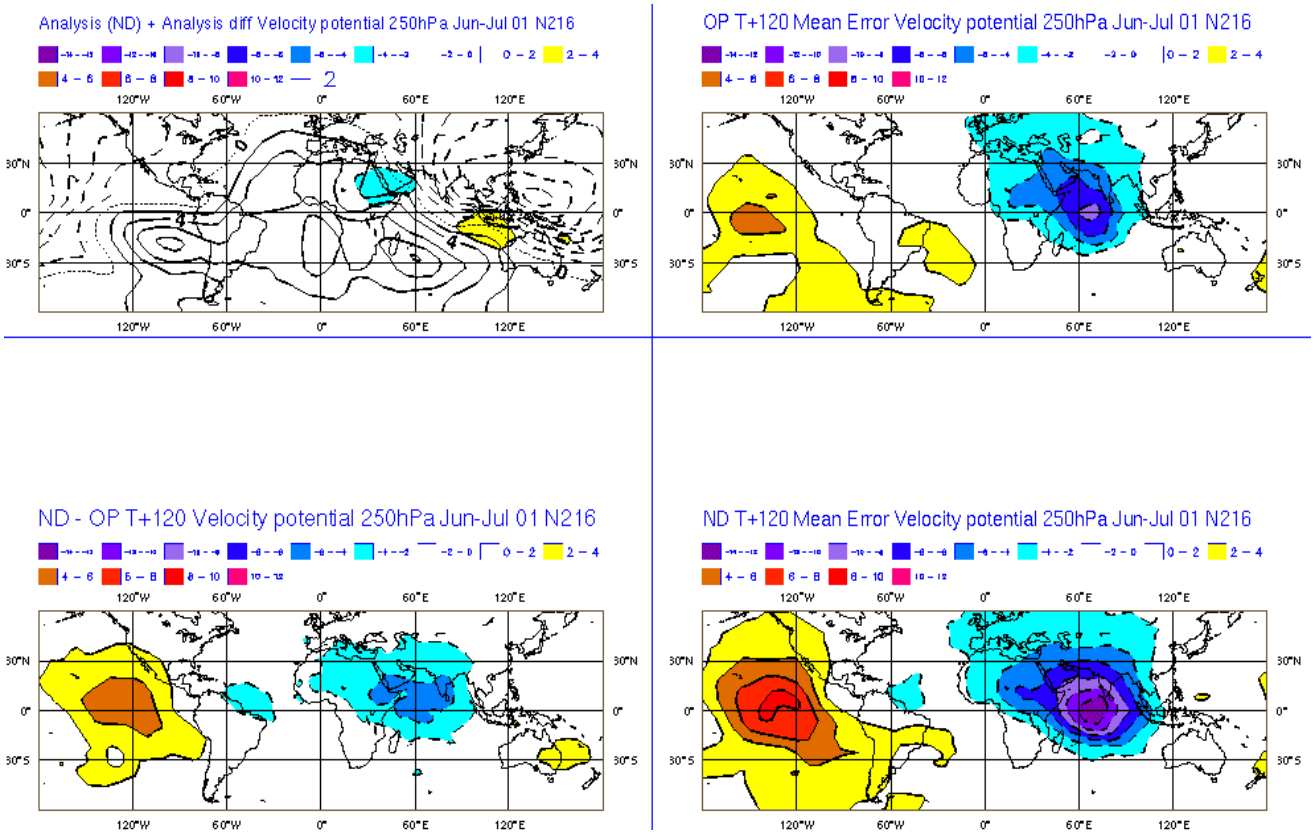

Figure 14: *250hPa velocity potential showing G27 analysis and analysis differences (top left), forecast differences (bottom left) and errors from each model's own analysis (top and bottom right) for T+120 Jun-Jul 01 trial.*

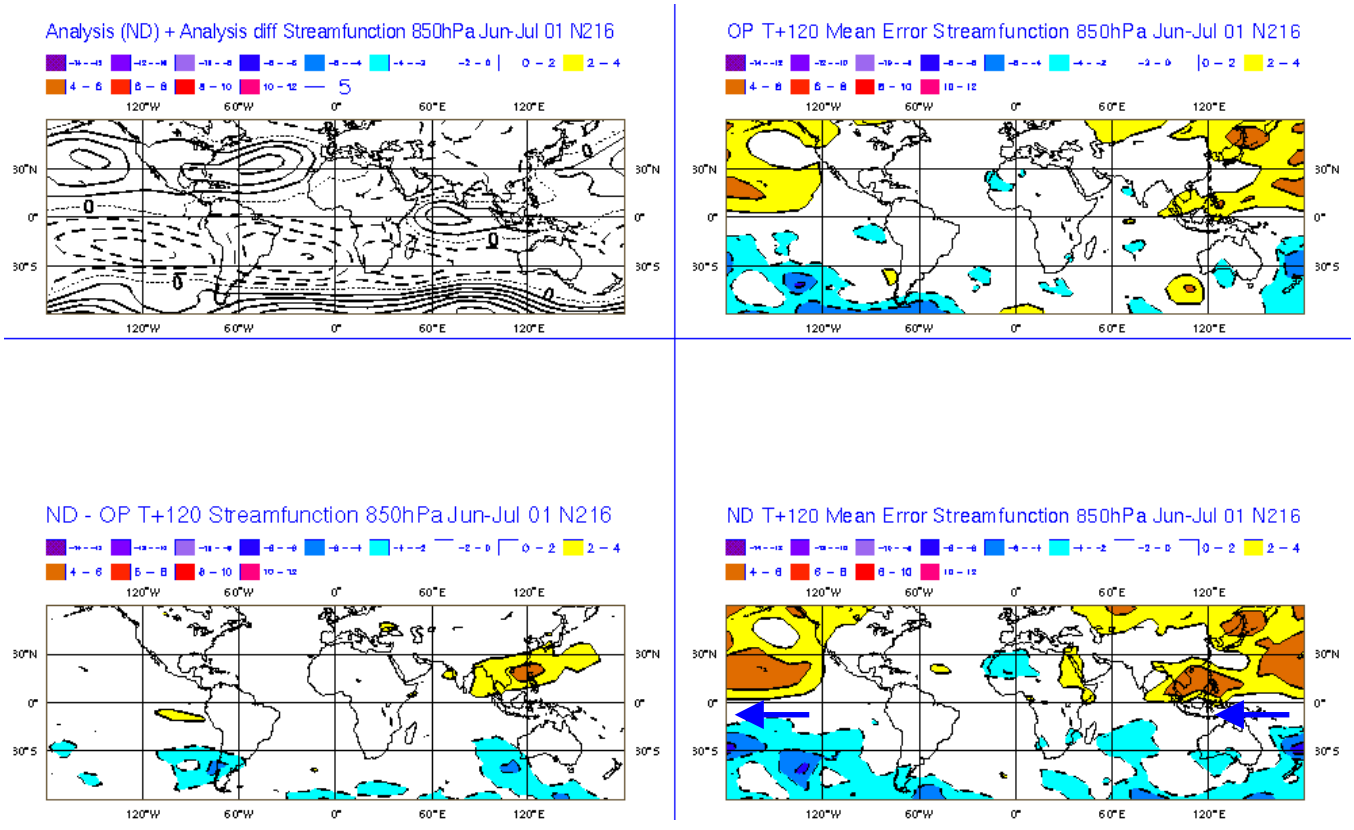

Figure 15 - as figure 14 but for 850hPa streamfunction

Pacific establish themselves within the first day of the forecasts and continue to grow up to day 5. There is a direct parallel with the tropical errors noted in the HadGEM1 climate version of the Unified Model currently under development. In these simulations we see increased low level easterly flow over the equator and increased wind stresses. In the coupled model there is a pronounced cold error in SST's along the equatorial Pacific, which tends to shut off convection on the equator. These cold SST's may be directly linked to excessive upwelling of colder water in the Pacific Ocean as a response to the increased wind stresses there. At 250hPa the signal is more mixed, but there are increased westerlies in the Pacific (not shown).

There is little evidence of a Rossby wave response to the west of the increased divergent flow at 850hPa (or 250hPa). The forecast differences (G27-G26) show that the main circulation changes occur to the east of the increased divergent flow in the Indian Ocean, with twin anticyclonic circulations over SE Asia and SW Australia at 850hPa (Fig. 15), and corresponding increased cyclonic circulations at the same locations at 250hPa (not shown). This latter response is qualitatively consistent with a Kelvin wave response and increased low level easterlies to the east of the heating predicted by the Gill-Matsuno model and was also found in tropical heating experiments with a resting stratified (baroclinic) atmosphere conducted by Jin and Hoskins (1995). They also found a planetary Rossby wave response to the west of their heating in the resting case. However, on introducing more complex basic states (3D time mean flows) they found considerable variability in the positioning and magnitude of the upper level anticyclones (Rossby wave response), perhaps consistent with our results.

5.4. Time-space variability of tropical wind errors - Hovmoller plots

Finally, we examine the time and space variability in T+24 tropical wind errors using Hovmoller plots. For the 850hPa velocity potential we can clearly see the signature of increased convergence in the Indian Ocean and divergence over the east Pacific in the G27 forecasts (Fig. 16). This signal is very systematic across all forecasts in our Jun-Jul trial. Consistent with this is a region of enhanced easterly error in the 850hPa zonal wind (Fig. 17). This is to the east of the main area of increased convergence, and is also very systematic across all forecasts.

6. Diabatic Heating and Temperatures

Given the major role played by diabatic heating in tropical circulations it is useful to look at this quantity in the G27 and G26 forecasts.

6.1. Heating increments from the models.

In this section we consider the thermal balance (dynamics + parametrized heating) from a 1 day forecast of G27 and G26 for a case in March 2001. The 24 hour increment fields and the overall budget residual (dynamics + parametrized heating) should give an indication of the drift from observations of each model's thermodynamic state and the possible roles played by each model routine in this drift (radiation, convection etc.). In addition, we have also run G27 without the 4A convection scheme (CMODS6) in order to see its impact on the diabatic heating field. There are two caveats to these results. Firstly, a case in March cannot be directly equated to errors in the Jun-Jul forecasts discussed in previous sections. Secondly, all the forecasts are run from an initial analysis of cycle G26. Clearly in addition to adjustments from the observed state there will also be an additional adjustment in the G27 forecasts from this G26 initial state where observations are sparse. Despite these caveats we believe the results are still informative about gross differences in the diabatic heating between G27 and G26.

The zonally averaged heating increments from each model routine are shown in figures 18 to 23. The results are summarised below.

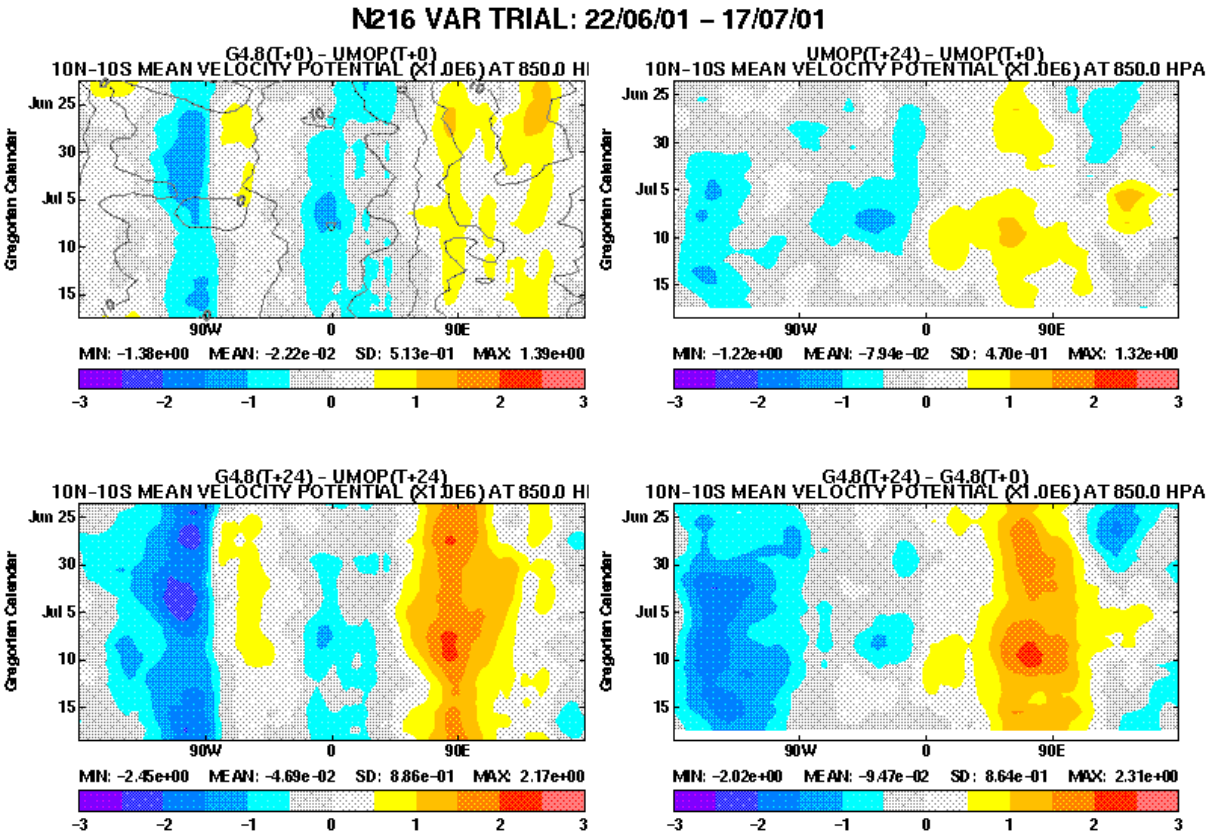

Figure 16 - *Hovmoller plots (time - longitude) of 850hPa Velocity potential showing G26 analysis and analysis difference (top left) and forecast differences (bottom left) and errors from each model's own analysis (top and bottom right) for T+24 Jun-Jul01 trial.*

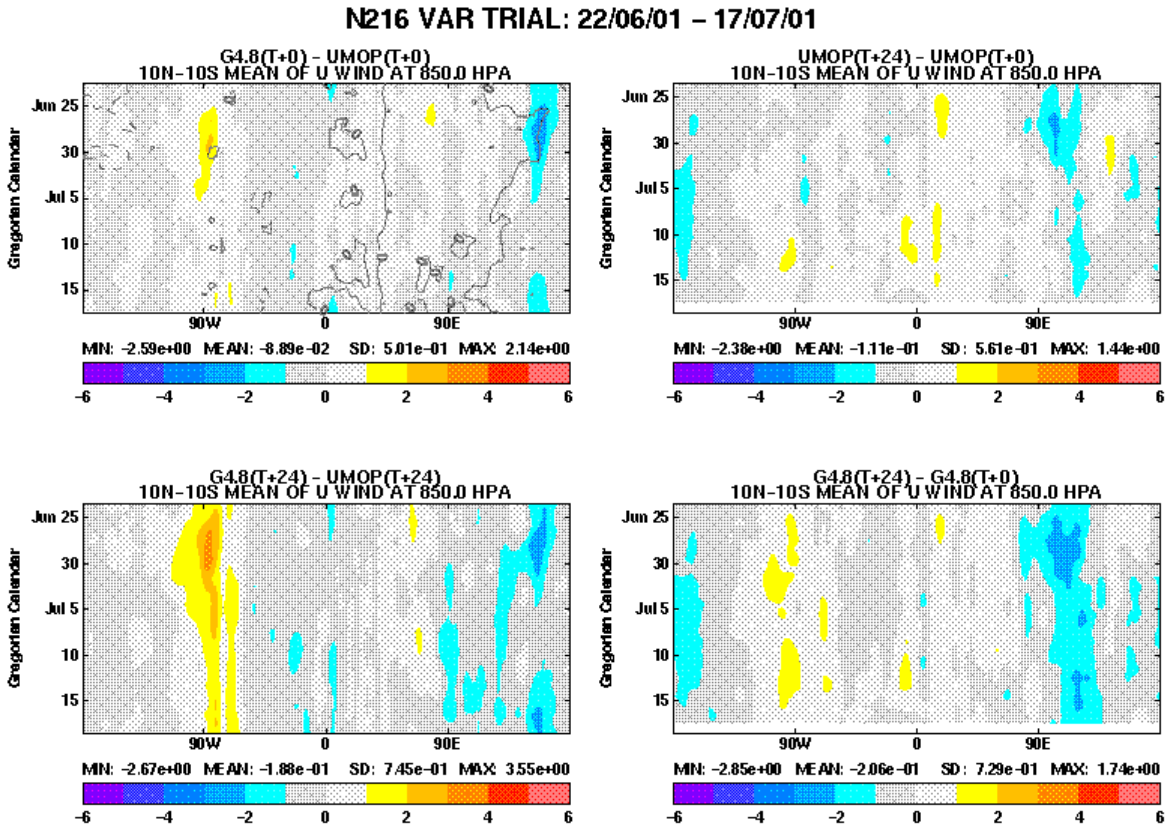

Figure 17: *As figure 16 but for 850hPa zonal wind*

- ***Convective heating (Fig. 18)*** - G27 has increased convective heating in the deep tropics compared to G26. Taking this result in isolation it is difficult to draw too many conclusions, as the increased convective heating may be transient adjustment of the G27 forecast from the G26 initial state. However, removing the 4A convection scheme does reduce the convective heating and this sensitivity suggests that details of the convective parametrization itself are important in determining the higher heating rates.
- ***SW radiation (Fig. 19)*** - The G27 versions show increased SW heating of the tropical mid-troposphere and sub-tropical boundary layer. The SW heating at the tropical tropopause is reduced in G27 compared to G26 and spread over a deeper layer. This latter response is probably a reflection of the very different convective cloud fractions arising from the use of anvils in G27 (Fig.36). The increased SW heating in the subtropical BL in G27 may be linked to increases in both layer and convective cloud fractions (Fig. 35 and 36 respectively).
- ***LW radiation (Fig. 20)*** - Overall a reduced LW cooling of the tropics and subtropics in G27 forecasts, apart from in local regions in boundary layer due to increased layer cloud (Fig.35) and convective cloud (Fig. 36). There is reduced cooling of the stratosphere in G27.
- ***Total radiation (Fig. 21)*** - less radiative cooling in the deep tropics and the subtropics in G27 compared to G26.
- ***Total parametrized heating (Fig.22)*** - Increased warming in G27 in the deep tropics (increased convective heating and reduced radiative cooling) and in the subtropical BL (reduced radiative cooling).
- ***Dynamical heating increments (not shown)*** - largely balance the parametrized terms, implying more vigorous ascent and adiabatic cooling in the deep tropics for G27. In the subtropics there is increased warming from the dynamics in the mid-troposphere associated with increased large-scale subsidence.
- ***Total temperature increment (Fig.23)*** - G27 has a warmer tropical and subtropical mid-troposphere than G26 (contributions from convection and radiation in the deep tropics and radiation and dynamics in the subtropics). Verification shows that G27 has a larger warm bias than G26 in this region (see next sub-section).

In summary, the G27 forecasts appear to have an increased warming tendency of around 0.5K/day in the mid-troposphere from 30N to 30S. In the deep tropics an increased convective heating and reduced radiative cooling in G27 relative to G26 appear to contribute to this warming. More vigorous ascent and adiabatic cooling from the dynamics attempt to balance this overall increased diabatic heating. Removing the 4A convection scheme reduces the diabatic heating and the residual warming tendency.

6.2. Temperature biases in the tropics.

Verification against sondes in the tropics shows that at T+120 the G27 forecasts have a mid-tropospheric warm bias of ~1K compared to 0.5K in the G26 forecasts (Fig.24). This is consistent with the warming tendency of the tropical mid-troposphere noted in the previous section. The RMS errors of temperature are also larger in the mid-troposphere in G27 (Fig.24). Using equation 1 we estimate that ~85% of the increase in RMS error can be attributed to the increase in the bias. In the stratosphere the large cold bias in G26 of -5K at T+120 is reduced to -1K in the G27 runs (Fig.24). The RMS errors in temperature are also reduced in the stratosphere (Fig. 24).

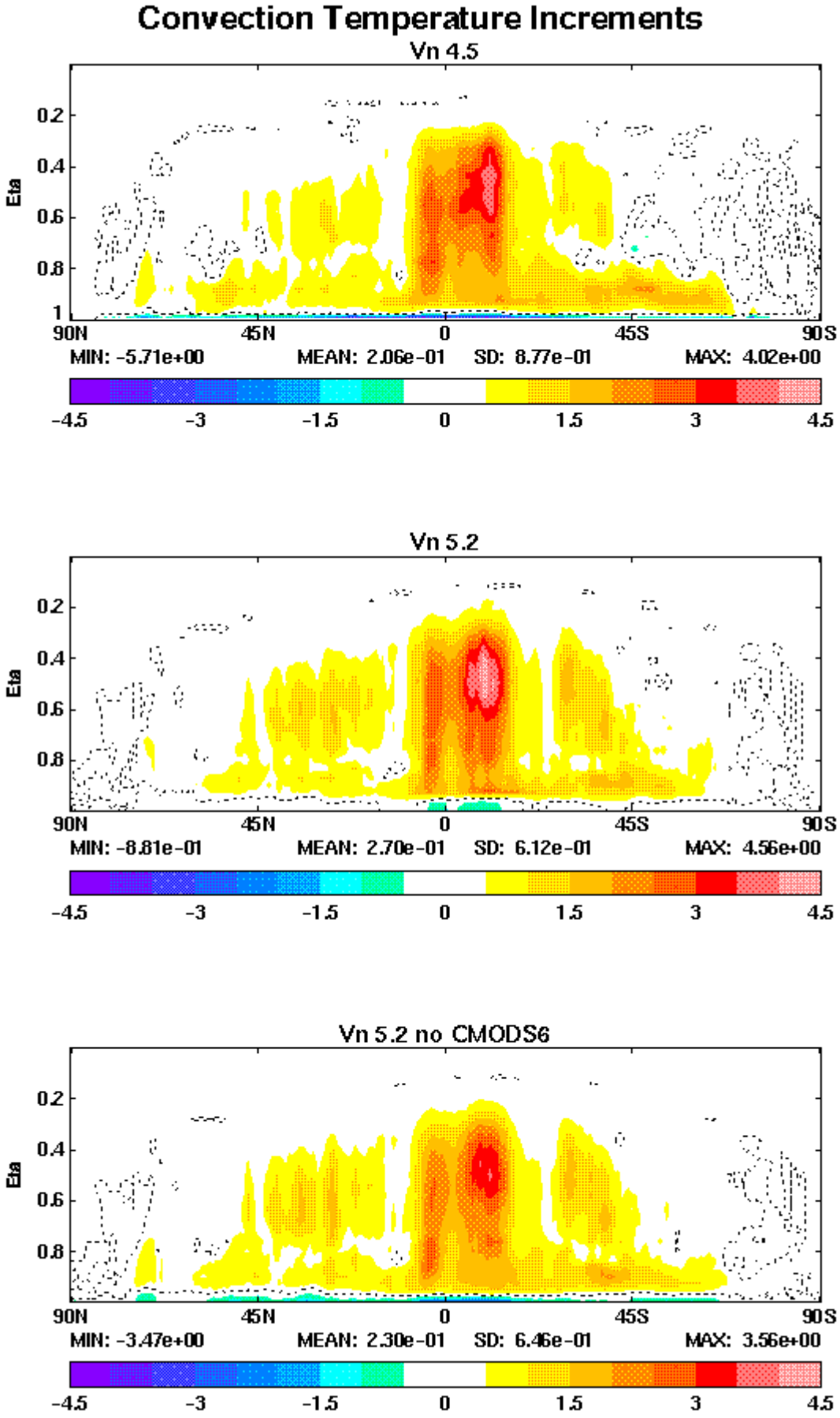

Figure 18: *T+24 daily averaged Convective heating increments (K/day) from a March 2001 case study showing G26 (vn4.5) (top) and G27 (vn5.2) (middle) and G27 without CMODS6.5 (bottom).*

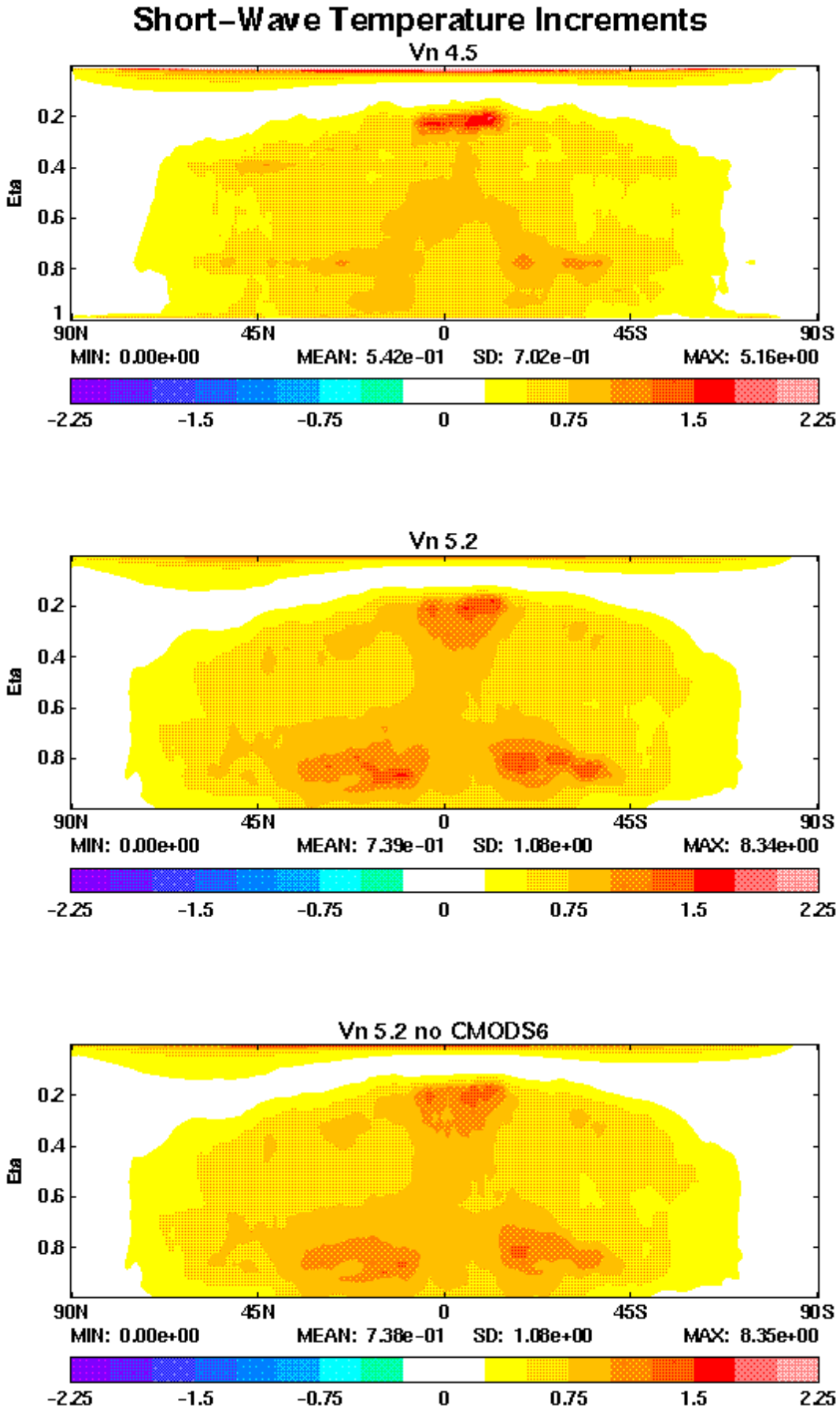

Figure 19: *as figure 18 but for SW radiative heating increments*

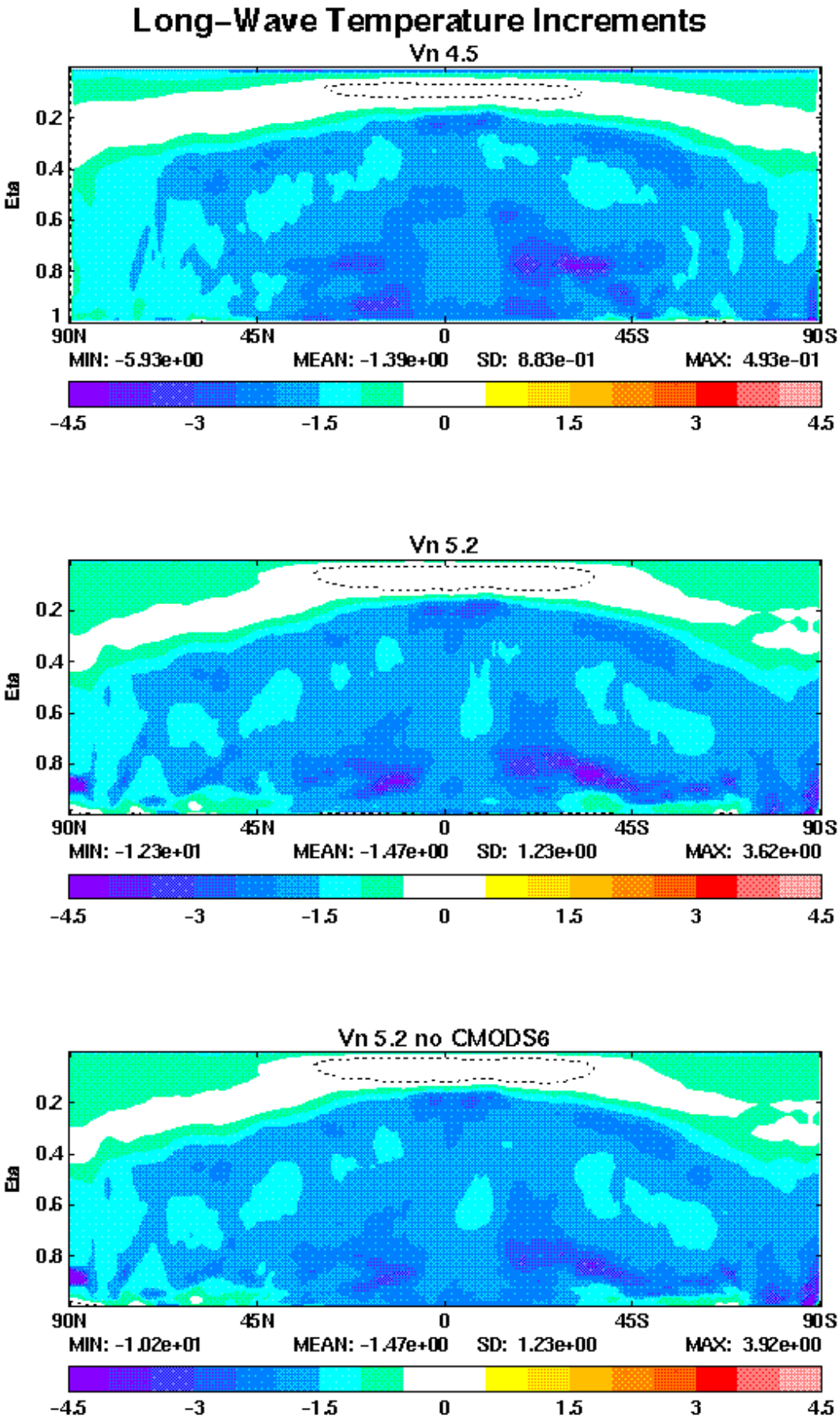

Figure 20 *As figure 18 but for LW radiative heating increments.*

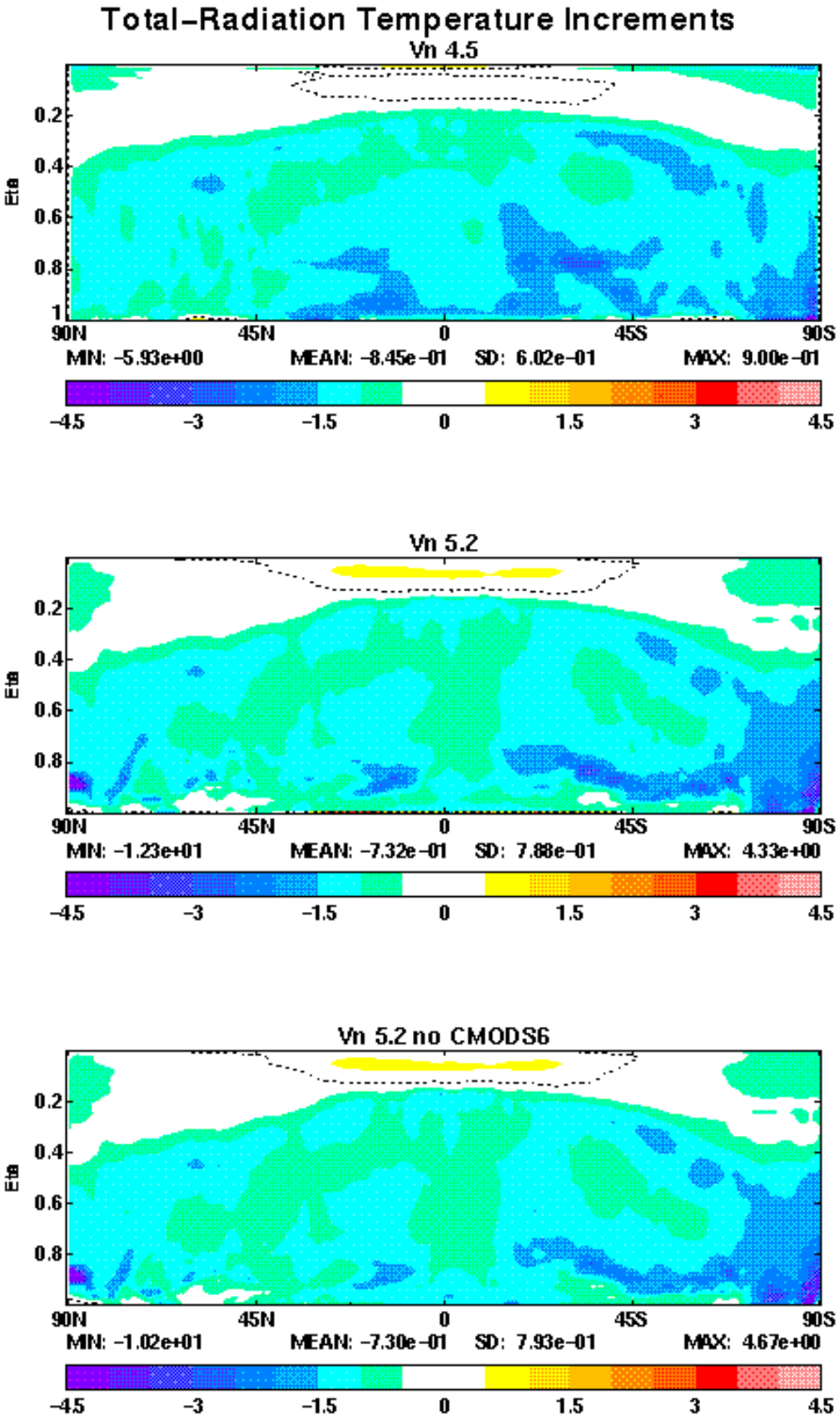

Figure 21: *As figure 18 but for Total (LW+SW) radiative heating increments.*

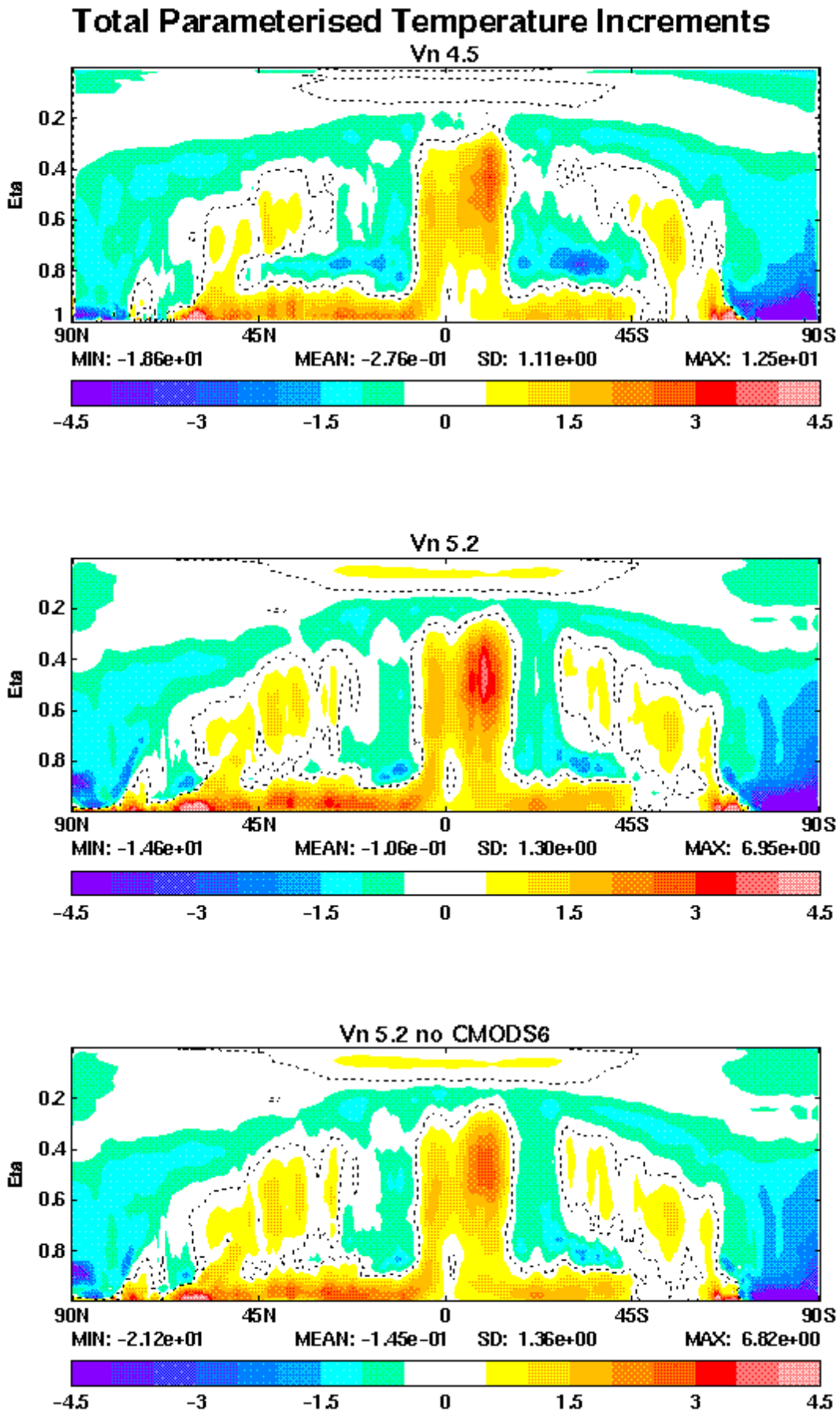

***Figure 22**: As figure 18 but for total parametrized heating increments.*

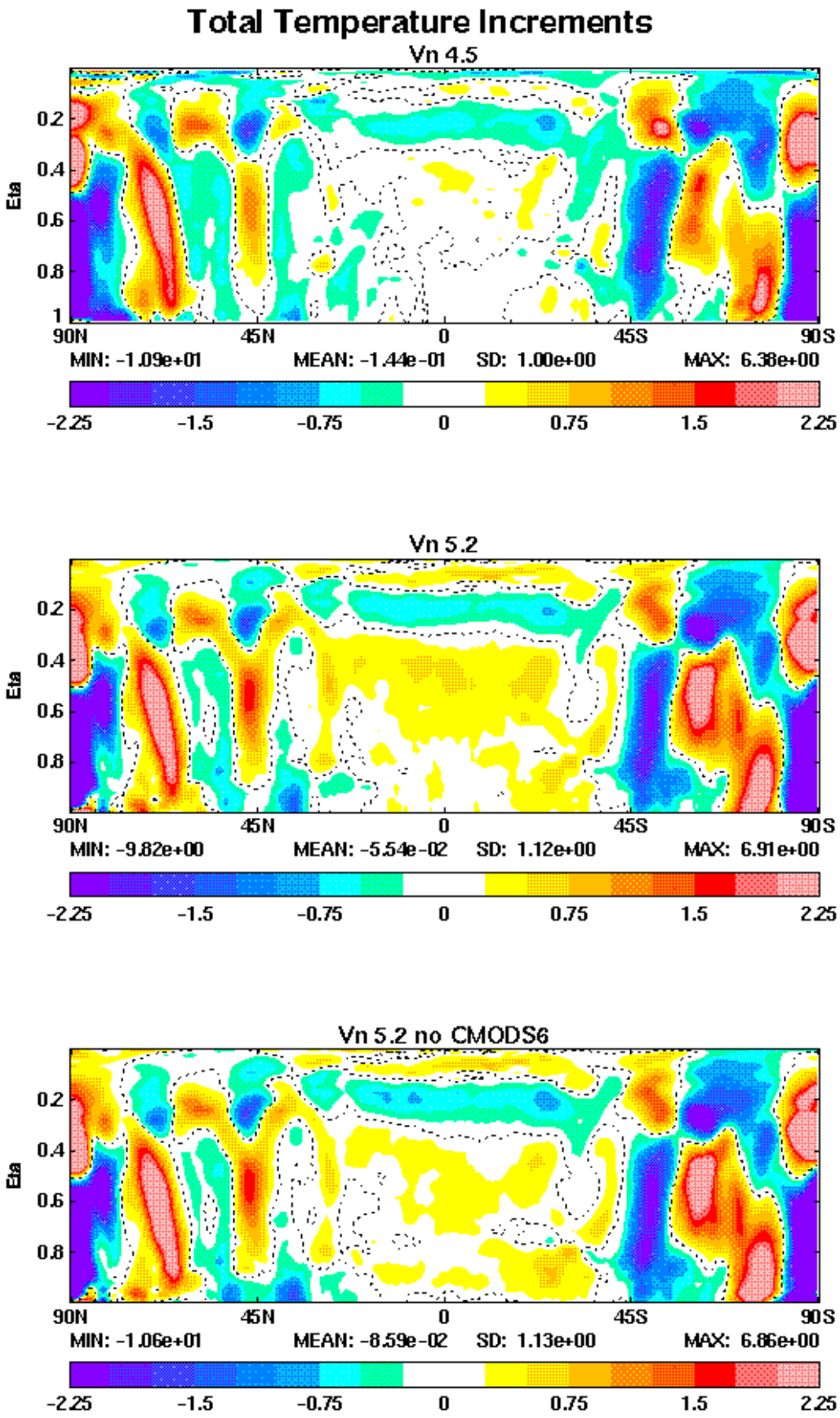

Figure 23: *As figure 18 but for total temperature tendency.*

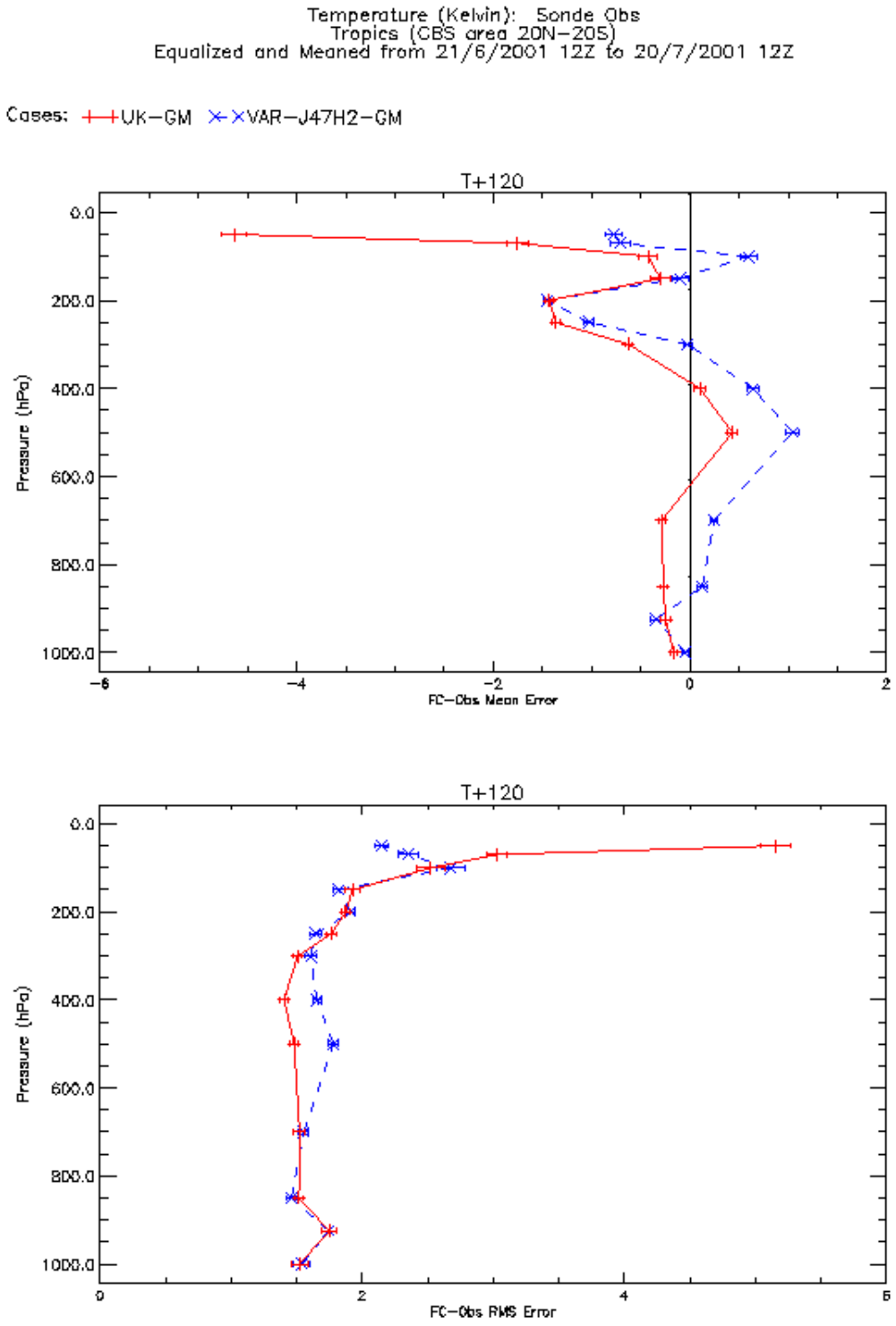

Figure 24: *Objective verification vs. sondes for T+120 temperature forecasts over the tropical domain (20N-20S) from Jun-Jul 2001 trial. Top panel shows the temperature bias and the bottom the temperature RMS error. G26 (solid red) and G27 (blue dashed)*

7. Sensitivity Tests - Impacts on tropical performance

In this section we consider the impact of a number of sensitivity tests that were carried out in order to try and understand the tropical performance. These included

- The impact of the 4A convection scheme (CMODS6) - see section 3 for description.
- Intermediate Edwards-Slingo radiation - this was an attempt to make the radiation scheme behave more like that in the G26 model, although it was never a scientifically credible alternative to the full E-S radiation. In more detail, for the LW: transmissivities for H_20 from the same source data as used in G26erational radiation scheme. O_3, CO_2, H_20 species and non-spherical ice included. Trace gases are neglected (CH_4, CFCs and N_2O). For the SW: As HadAM4, including non-spherical ice but no aerosol.
- Vertical diffusion in the tropics (30N-30S)

The diagnostics are from a series of Nov-Dec 1999 trial runs at N144 resolution carried out as part of the evaluation the performance of the New Dynamics and HadAM4 physics.

7.1. Tropical wind verification

Figures 25 and 26 show the impacts of 4A convection and Intermediate E-S on the 850hPa and 250hPa tropical wind error growth curves.

At 850hPa the inclusion of the 4A convection scheme made a major improvement to RMS vector wind errors, making the G27 error growth very similar to that in G26. The mean speed error was changed from a positive error of 0.8 m/s at T+120 to a negative error of -0.3 m/s, comparable in magnitude (but not sign) with the G26 error. The main contribution to this improvement came from the change in the closure of the convective momentum transports implemented as part of the 4A convection. Including the intermediate E-S scheme had a smaller but positive impact on both wind speed errors and RMS vector wind errors relative to the control runs of the G27 (see figure caption).

At 250hPa the intermediate E-S radiation makes a reduction in the RMS vector wind errors, closing the gap between the benchmark run of the new Unified Model (see figure 25 caption) and G26 by almost a half at T+120. However, adding the 4A convection package in on top of the radiation actually makes 250hPa wind error marginally worse again at longer forecast ranges.

7.2. Eddy kinetic energy

The new Unified Model without the 4A convection package showed a distinct increase in eddy kinetic energy (EKE) over equatorial regions in lower and upper troposphere compared to G26 (Fig. 27). This gives larger errors in EKE (Fig. 27 - right panels). Including the 4A convection package alone gave a clear reduction in the low level EKE and some improvement in the upper levels, although the EKE at 250hPa was still higher than G26. This is consistent with the impacts on 850hPa and 250hPa wind errors discussed in the previous section.

Adding the intermediate E-S radiation code also gave a beneficial reduction in upper and lower level tropical EKE (Fig. 27). However, this change also reduced the extratropical EKE in both hemispheres and increased the errors in those regions (Fig. 27 - right panels). This was one of the reasons the intermediate E-S radiation was not included into the operational version of the revised physics, despite its positive impact on tropical winds.

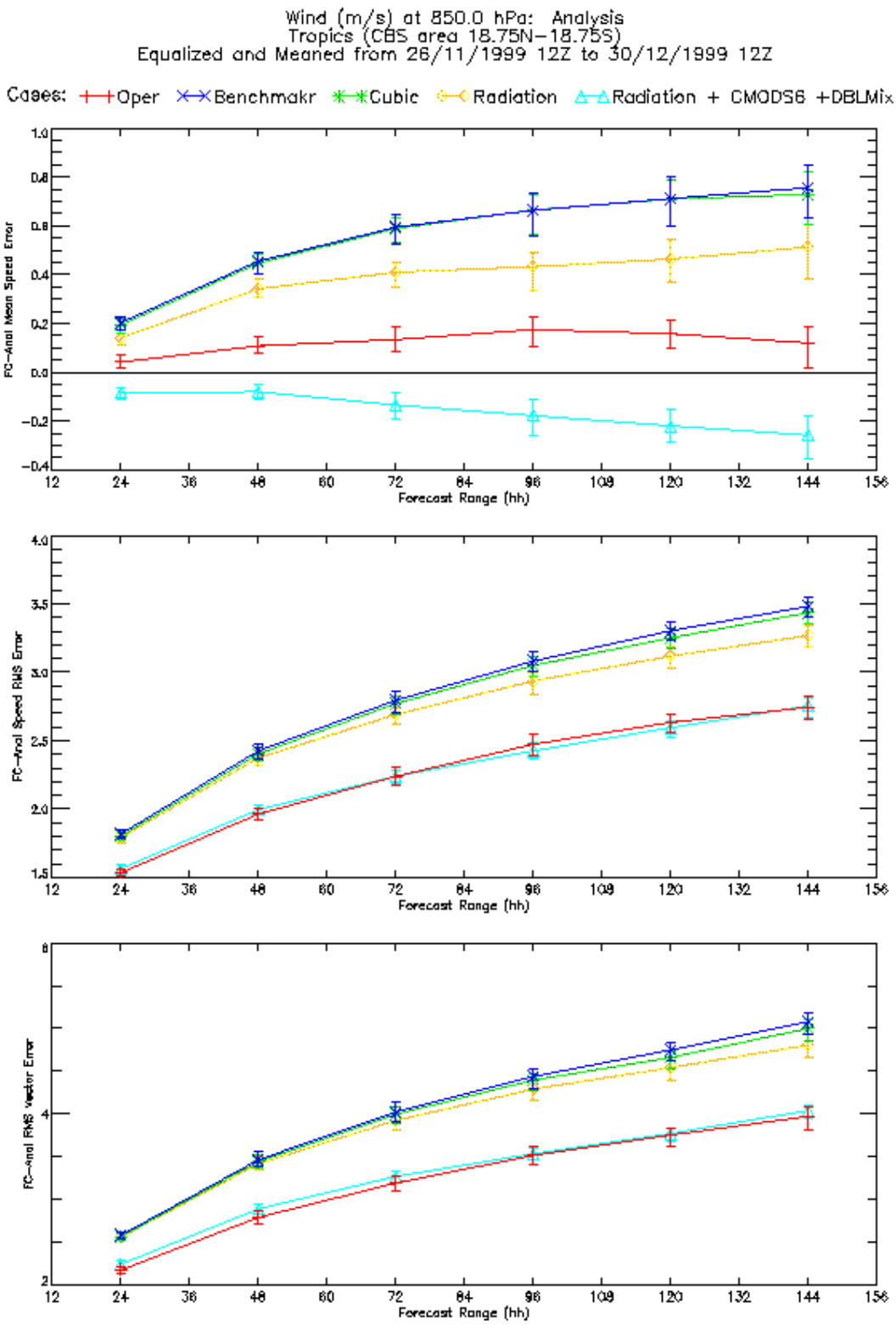

Figure 25: *Impacts of various N144 sensitivity studies on 850hPa tropical error growth curves (vs analysis). G26 (red), new dynamics and revised physics "benchmark" run (blue), "benchmark" + cubic interpolation (green), "benchmark" + intermediate E-S radiation (yellow), "benchmark" + CMODS6 + double asymptotic mixing length (turquoise). Mean speed error (top), RMS error in wind speed (middle), and RMS vector wind error (bottom). See text for more details of the experiments.*

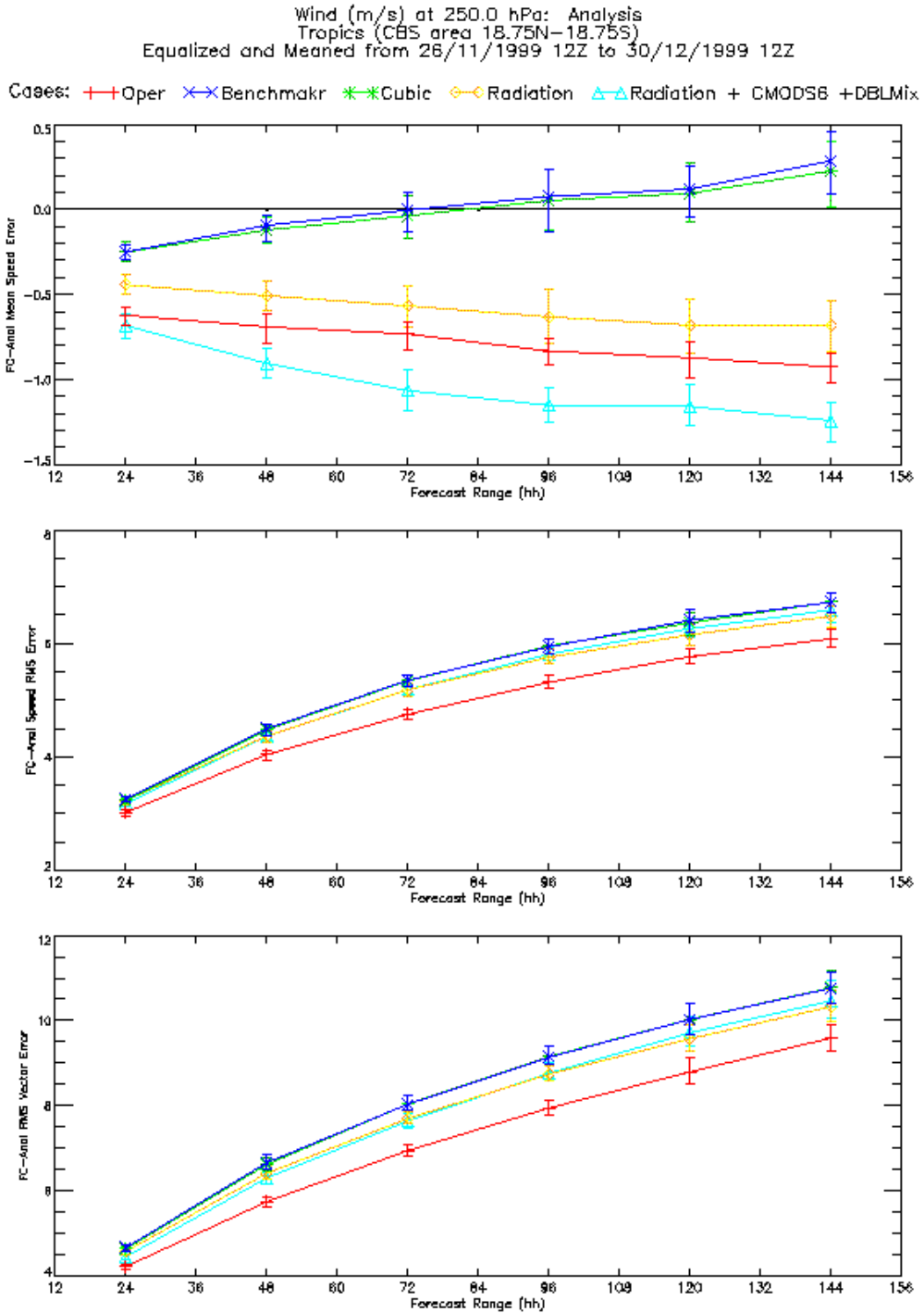

Figure 26: *as figure 25 but for 250hPa tropical winds.*

7.3. Zonally averaged temperatures

The impact of 4A convection on the temperatures is to warm the tropical mid-troposphere by up to 0.5K in 5 days (Fig. 28). This gives increased warm biases in the tropics as noted earlier. The 4A convection scheme also cools the subtropical boundary layer. The latter may be a radiative response to additional BL cloud in the 4A convection scheme (Fig. 35 and 36).

The intermediate E-S radiation warmed the upper troposphere in the subtropics (Fig. 29), but cooled the boundary layer by up to a degree in places, increasing the temperature error (relative to its own analysis). Although this radiation change was designed to make the G27 version perform more like the G26 model in terms of the basic radiation code, it cannot account for the fact that the cloud distribution in the G27 model is very different from that in the G26 model, particularly in the boundary layer (Fig. 35 and 36). It is likely that differences in the cloud-radiation interaction may be responsible for the poor performance of the intermediate E-S radiation in the boundary layer. Again, for this reason the intermediate E-S radiation was not included operationally.

7.4. Impact of vertical diffusion

The old operational version of the global NWP Unified Model (cycle G26 and earlier) have been run for many years with a vertical diffusion applied between 30N and 30S and between ~500 hPa and ~150 hPa (Wilson, 1992). Given our problems with 250hPa wind scores in the G27 version it was decided to try vertical diffusion in the new model. Figure 30 shows the impact on RMS vector wind errors of applying the vertical diffusion in G27 forecasts. At T+24 and T+120 the vertical diffusion acts to reduce the RMS vector wind errors over the layers 600-150hPa. At T+120 and 200hPa the difference in wind errors between G27 and G26 is reduced by ~30% by applying vertical diffusion. This was implemented into the operational version of G27. It is important that the sensitivity to vertical diffusion is re-assessed periodically as other improvements to the tropical circulation are made. In particular, a more complete assessment of the impact of vertical diffusion on tropical variability is required.

7.5. Grid-point storms

The original trial of 4A convection showed a marked increase in the number of gridpoint storms, as diagnosed using the maximum large-scale precipitation rate (Fig. 31). To counteract this a number of measures were taken including

- Introduce an RH based CAPE closure
- Introduce moisture diffusion

This has largely controlled fatal errors, although we still see occasions where precipitation rates are very high, suggesting we are only just controlling this problem.

8. Precipitation and Cloud

8.1. Precipitation

The precipitation from the full N216 trials are of limited use as they were only output as instantaneous rates and as such do not sample the full diurnal range. Instead we look at the evolution of 24 hour-accumulated precipitation from operational forecasts of G27. Figure 32 shows the T+00-24,T+48-72, and T+96-120 forecast ranges all verifying over the same 24-hour period of 00UTC 14th August to 00UTC 15th August 2002. Comparing the early and later

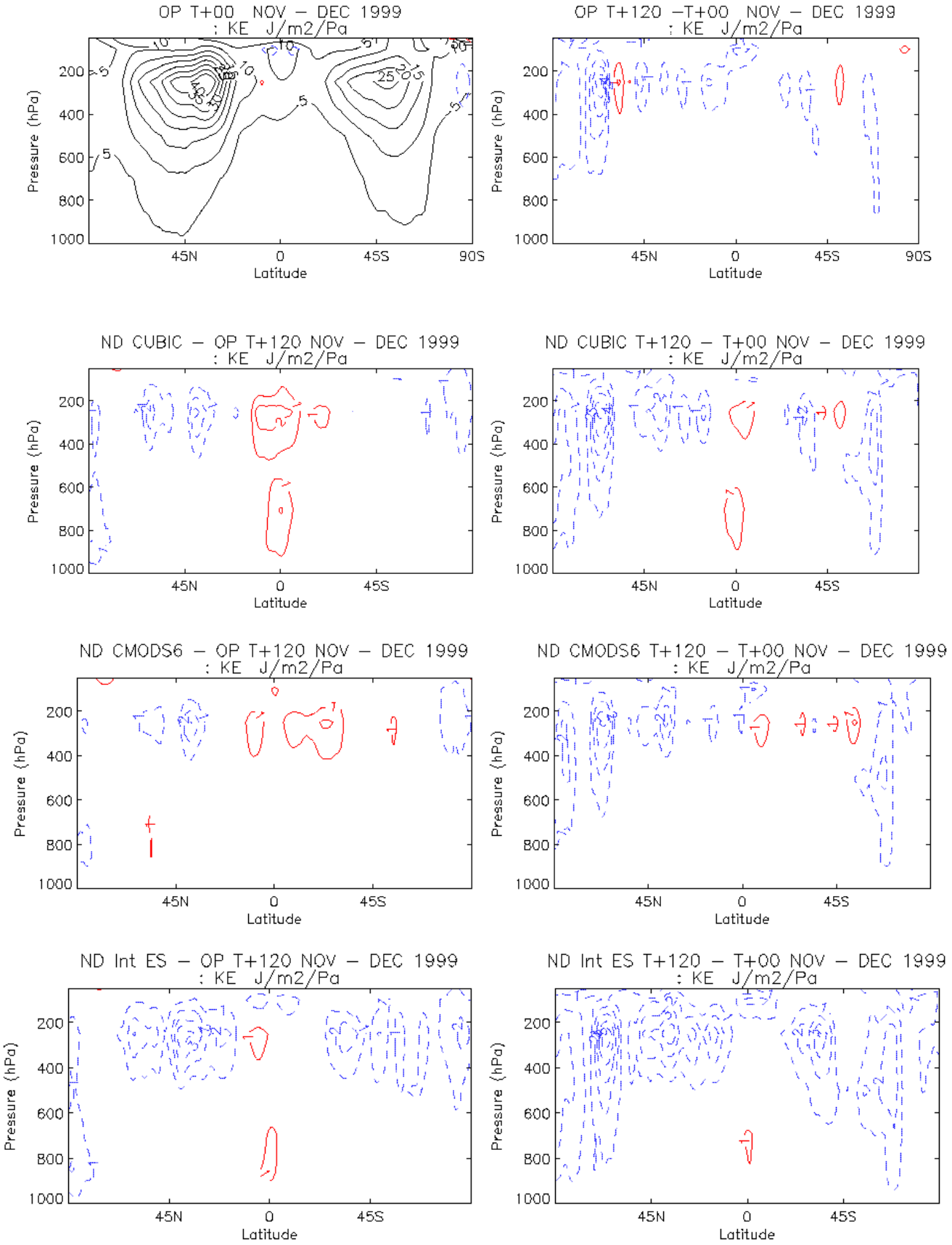

Figure 27: *Impact of various N144 sensitivity tests (Nov-Dec 99 trials) on zonally averaged eddy kinetic energy. Left column shows the G26 analysis and forecast differences of the new Unified Model sensitivity tests from G26. Right column shows the mean error (from own analyses) of G26 and various sensitivity tests (NewModel + cubic SL interpolation, New Model+cubic+CMODS6, New Model+cubic+intermediate E-S radiation)*

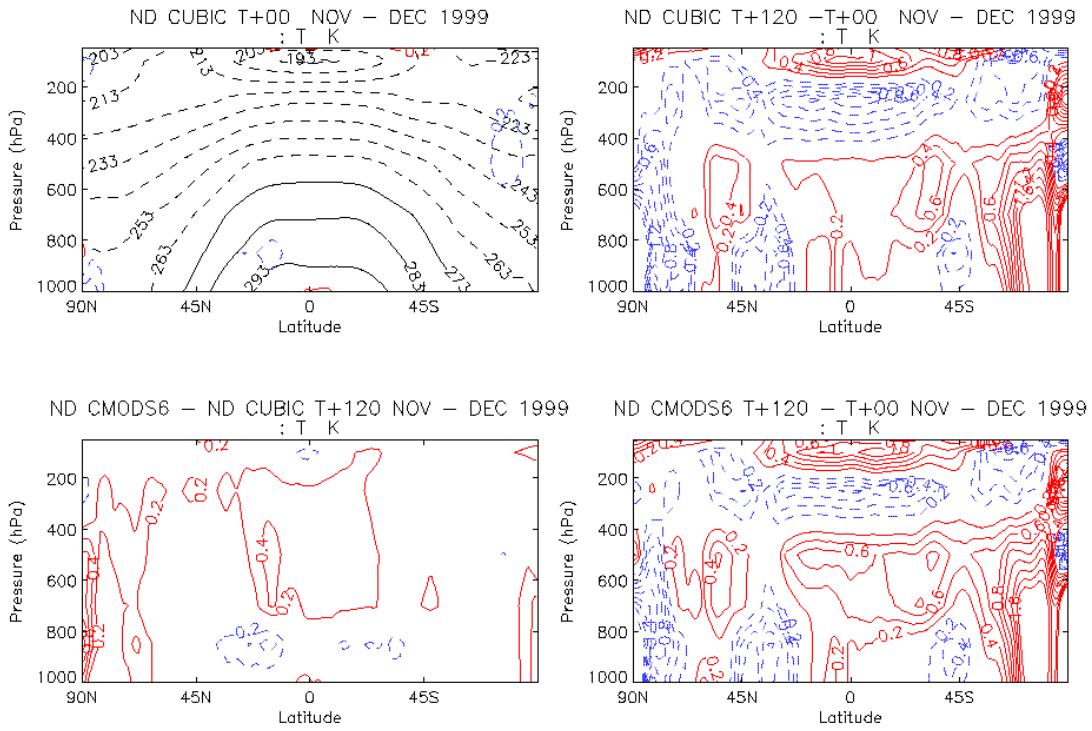

Figure 28 - *Impact of 4A convection (CMODS6) on T+120 temperature forecasts. Results from N144 Nov-Dec trials.*

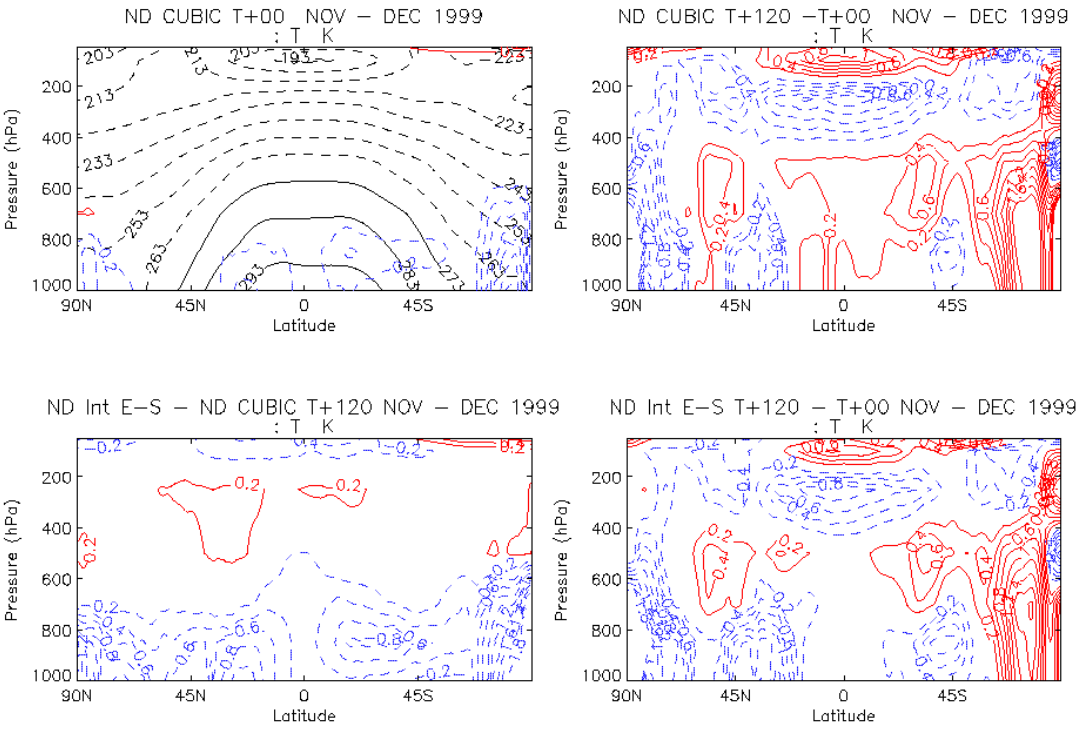

Figure 29 - As figure 28 but for the impact of intermediate E-S radiation on T+120 temperature forecasts.

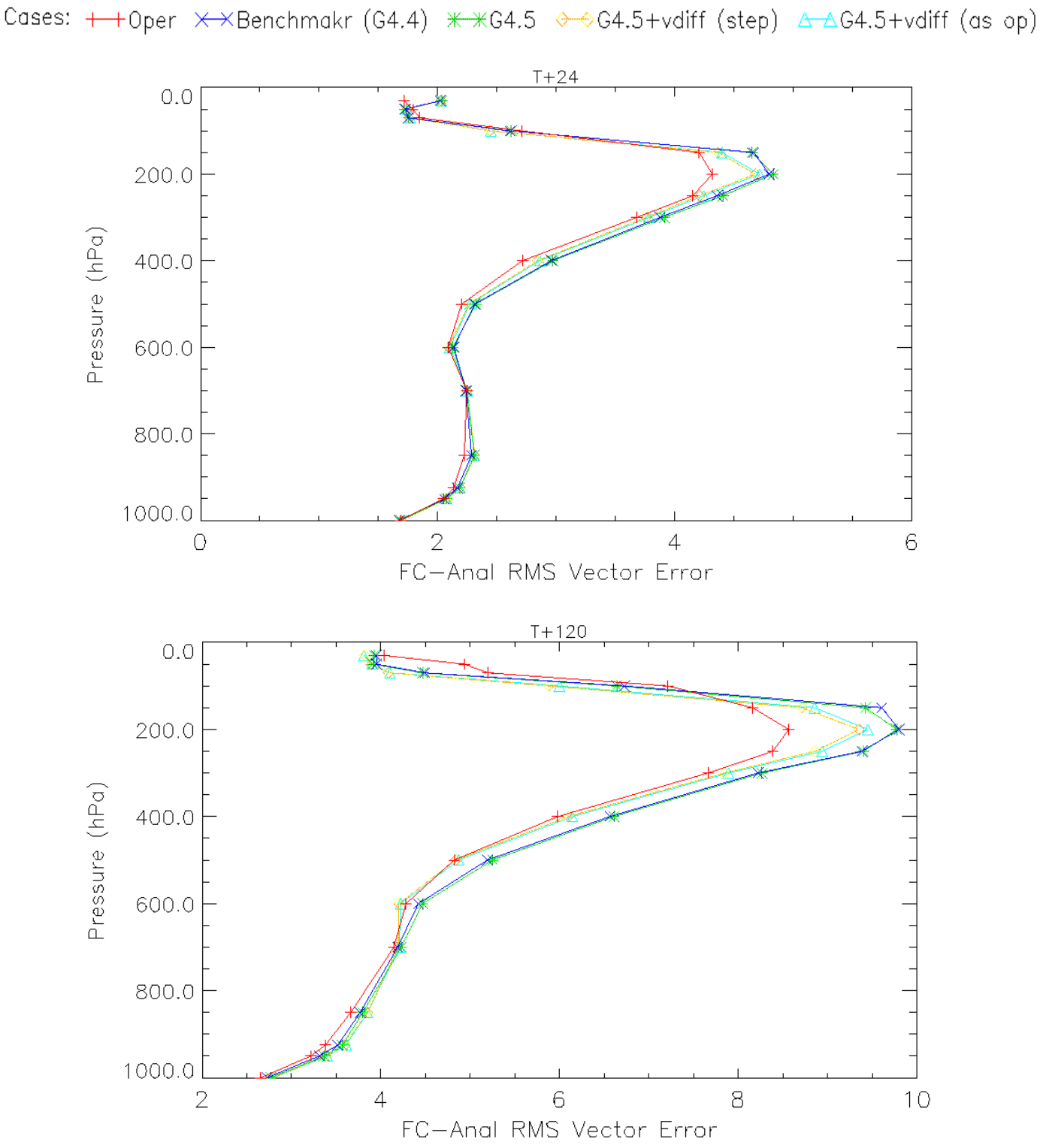

Figure 30: *The impact of applying vertical diffusion (yellow and turquoise curves) on the T+24(top) and T+120 (bottom) RMS vector wind errors. The yellow curve shows vertical diffusion applied with equal weight between 30N and 30S and zero outside this domain (i.e. step function in vdiff at 30N and 30S). The turquoise curve shows the impact of applying vertical diffusion as in G26 with a weighting function that tails off smoothly to zero at 30N and 30S.*

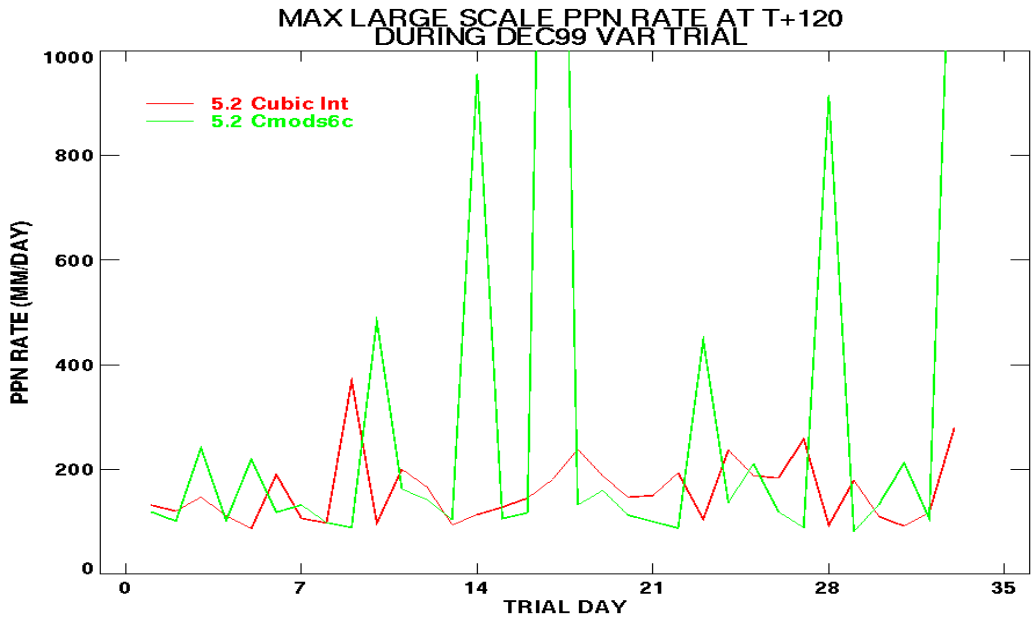

Figure 31: *Maximum large-scale precipitation rate in T+120 forecasts for N144 Nov-Dec 99 trials of New Model+cubic SL interpolation and New Model+cubic+Cmods6. This diagnostic is used as an indicator of gridpoint storms.*

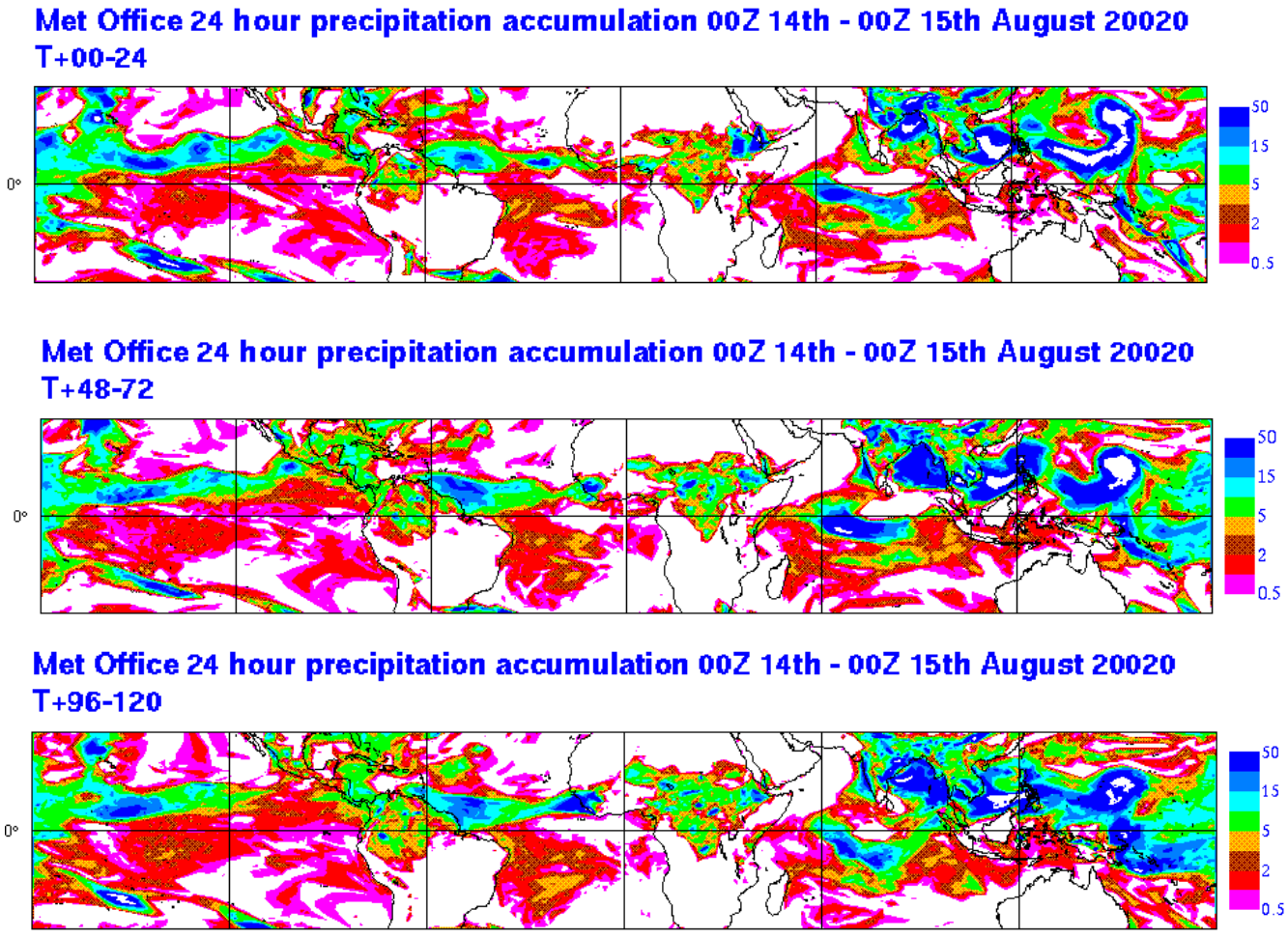

Figure 32: *24 hour precipitation totals (mm/day) for the period 14-15 August 2002 for the T+24, 72 and 120 forecasts verifying at that time. Forecasts are with cycle G27.*

forecast ranges we see an evolution generally consistent with errors in the divergent circulation (shown in Fig. 33). There is some evidence of increased precipitation in the vicinity of the Indian sub-continent (Bay of Bengal and the Western Ghats. In contrast we see a clear decrease in precipitation in the east Pacific consistent with the tendency for increased large-scale subsidence in this region (Fig. 33), which is clearly suppressing the convective activity. A similar error has been noted in the HadGEM project. Of course, these diagnostics only show the consistency between the drifts in precipitation and the divergent circulation and do not point to cause and effect.

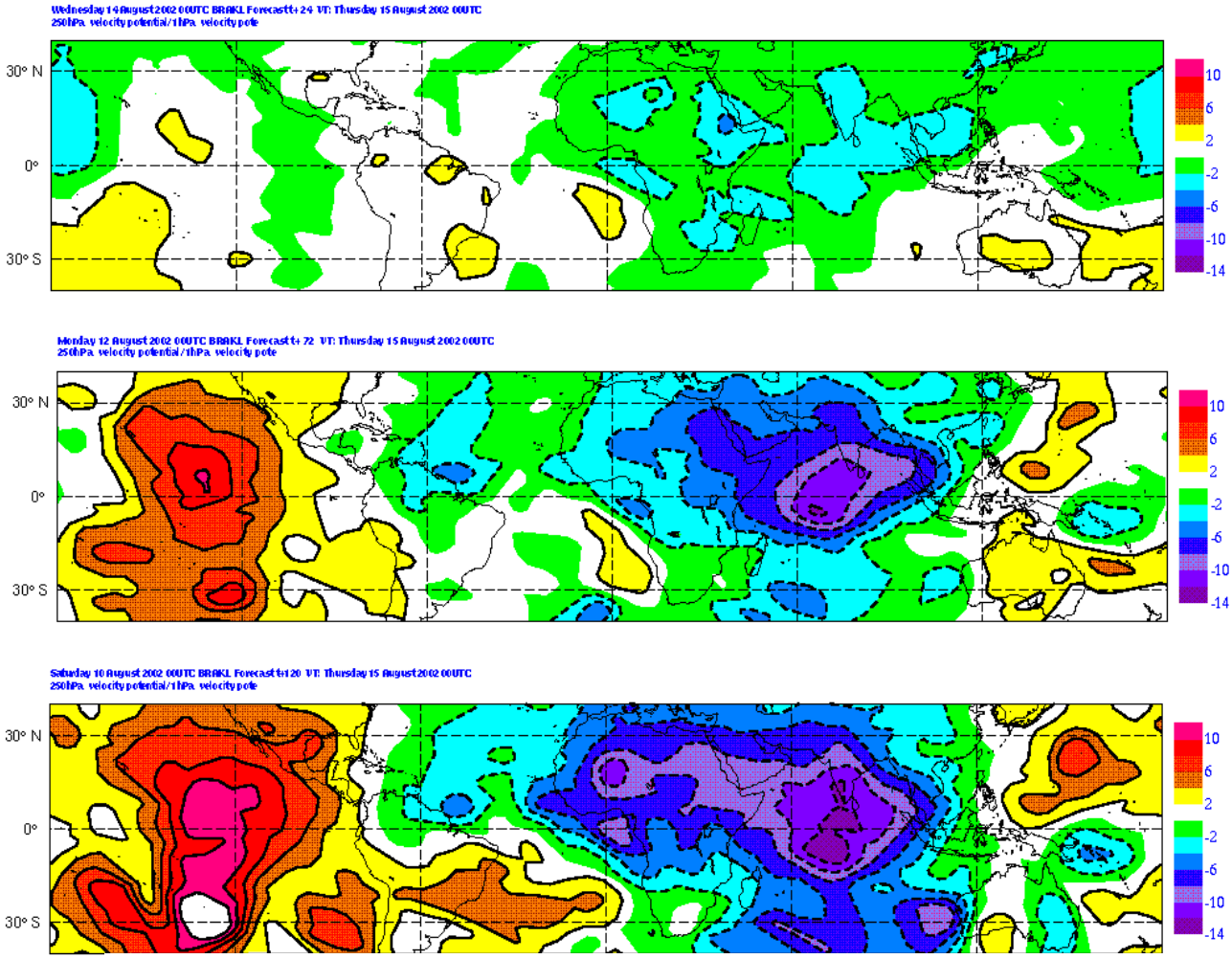

Figure 33: *The errors in 250hPa velocity potential for T+24,72 and 120 cycle G27 forecasts all verifying on the 15th August 2002 (negative => excessive divergence)*

8.2. Total cloud fractions

The total cloud fraction shows an increase in global cloud cover from 50% to 58% at T+24 for Jun-Jul forecasts (Fig.34). This is beneficial in the stratocumulus regions off the western coasts of S.America, Africa, and California, as can be seen in the reduction in positive errors in the TOA net downward SW radiation close to the coasts (Fig. 38). However, cloud tends to be too extensive in the trade-cumulus regions. The other large changes are in the extratropical stormtracks and over the North Pole. Similar increases are seen in the other seasons.

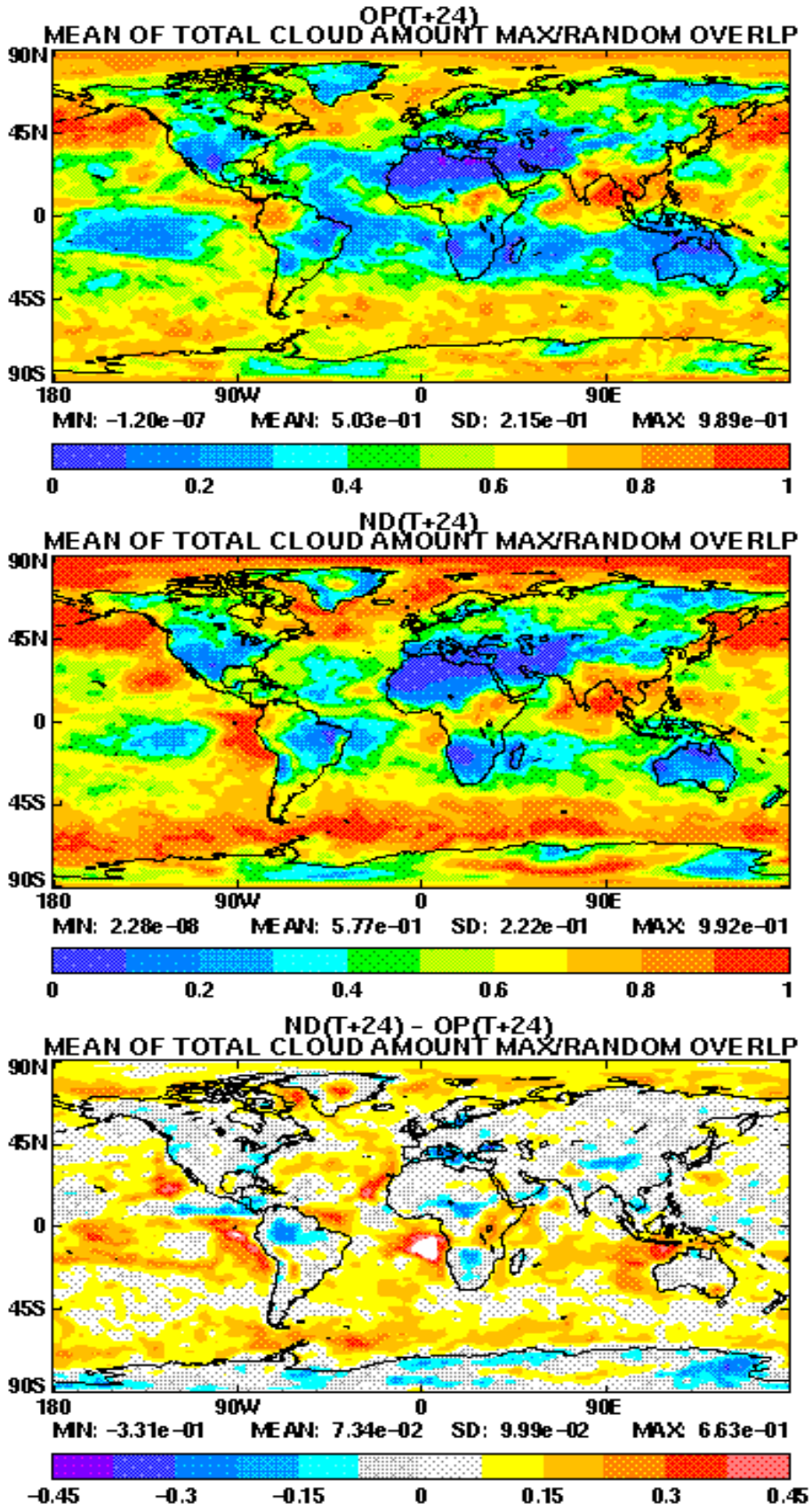

Figure 34: *Total cloud fraction (Max/Random overlap) for T+24 forecasts from the Jun-Jul 2001 N216 trial. G26 (top), G27 (middle), G27-G26 (bottom). The fields have been smoothed to accentuate the largest scales.*

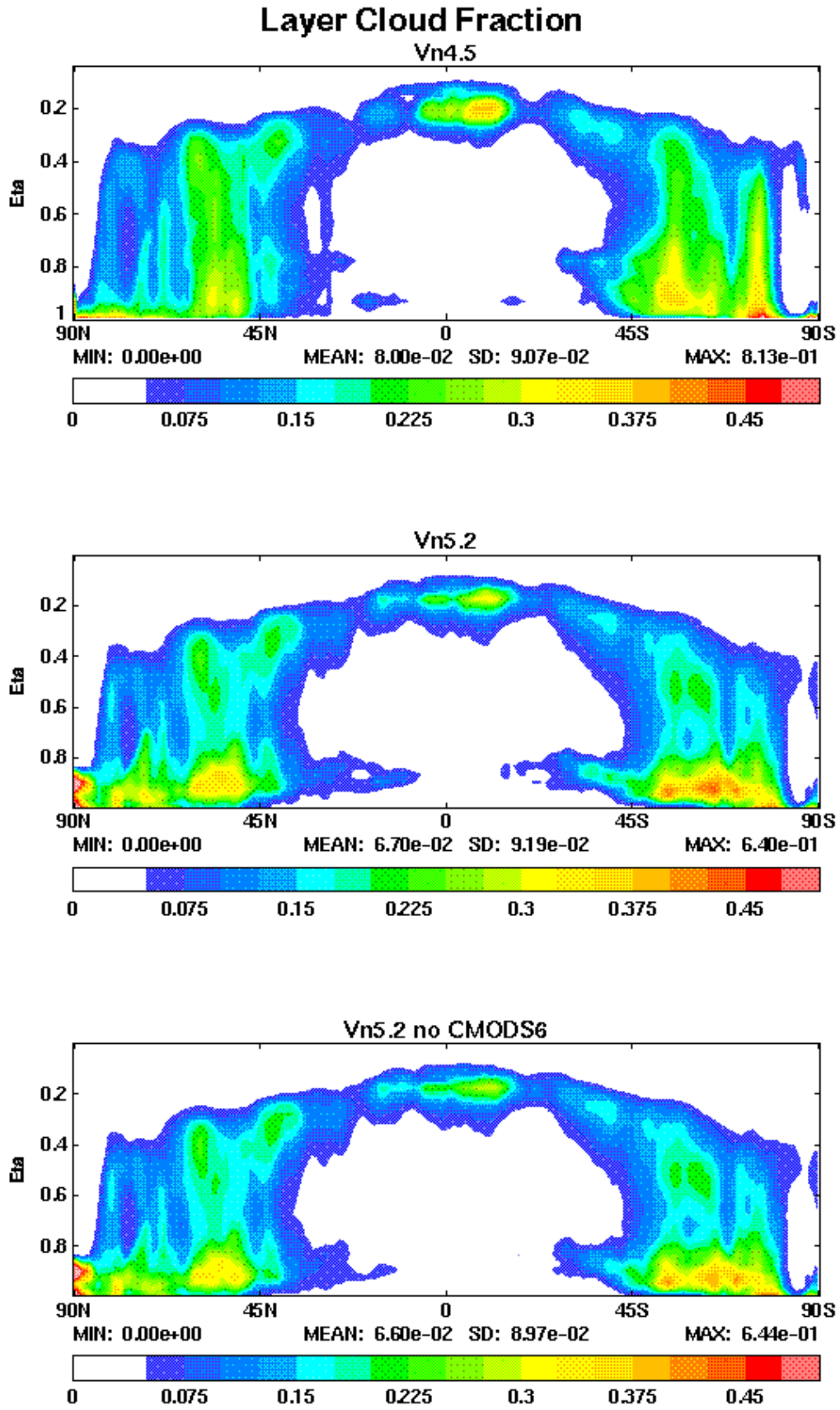

Figure 35: *T+24 zonally averaged layer cloud fractions from a March 2001 case study showing G26 (vn4.5) (top) and G27 (vn5.2) (middle) and G27 without version 4A convection (CMODS6) (bottom).*

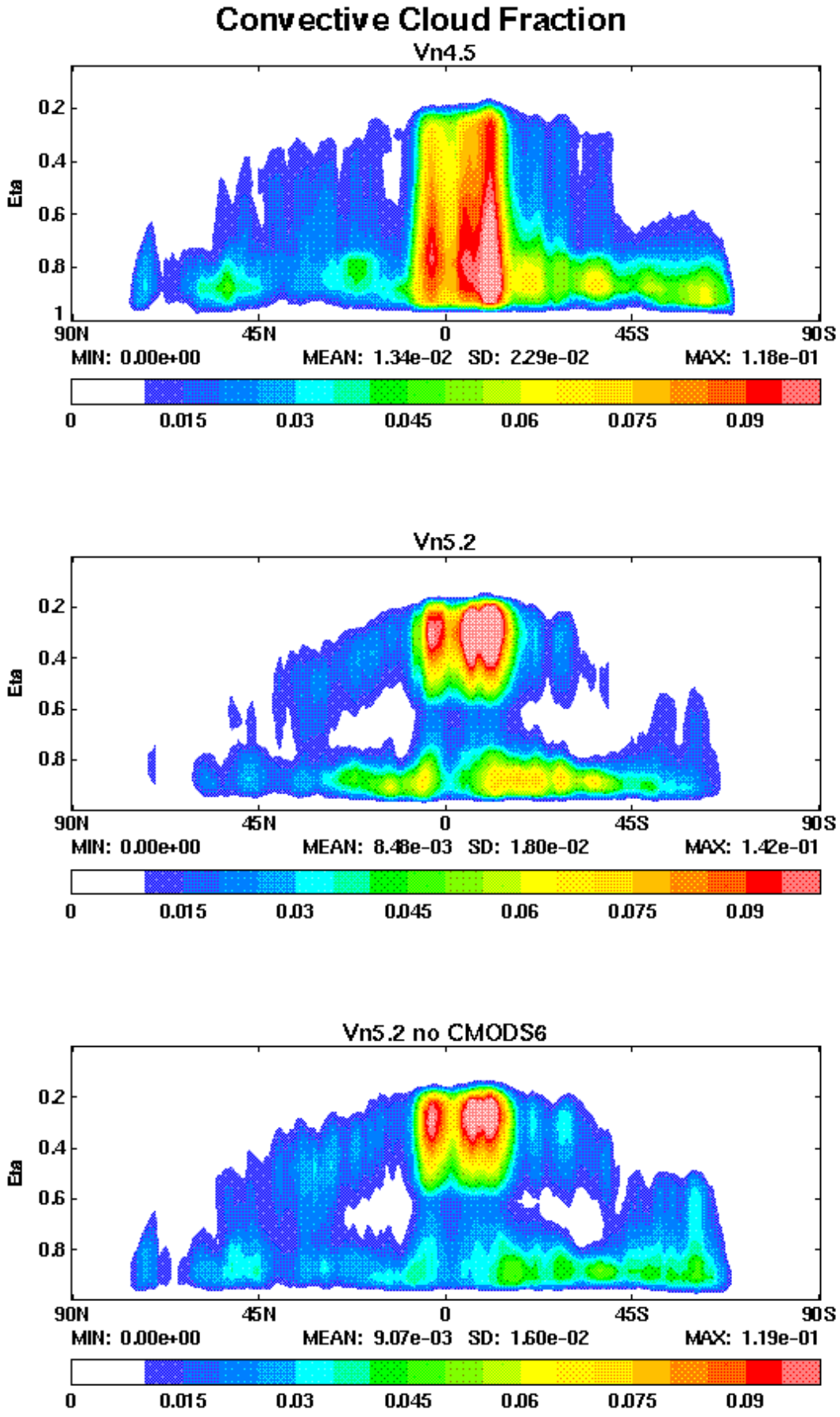

Figure 36 *- As figure 35 but for convective cloud fractions.*

8.3. *Zonally averaged cloud*

The main increase in cloud in G27 comes in the boundary layer (Fig. 35). There has actually been a decrease in mid-level and upper level cloud fractions. The major change in G27 convective cloud fractions comes from the redefinition of cloud into a tower fraction and an anvil fraction (Fig. 36). This has been shown to improve the top of the atmosphere radiative balance in climate versions (see section 8.4). Including version 4A convection scheme gives larger convective cloud fractions in the tropical and subtropical boundary layer, presumably associated with an explicit diagnosis of shallow convection. The impact of this low level cloud can be seen on the radiation increments of G27 with and without 4A convection, with increased SW heating (Fig.19) and increased LW cooling locally (Fig. 20).

8.4. *Top of the atmosphere radiation balance*

The global top of the atmosphere radiation balance is improved in G27 compared to G26, with large improvements in OLR which was previously too large in G26, and smaller improvements in the net downward SW fluxes (Table 1). Part of the improvements in OLR come from the use of the anvils in G27, which have reduced the large positive OLR errors that occurred in the G26 forecasts over the convective regions of Indonesia and Central America (Fig. 37). Over the oceans the G27 forecasts have consistently less net downward SW radiation than G26, in agreement with there being more bright BL cloud in G27 and hence more reflection of SW radiation back to space (Fig 38). Over land both models suffer from excess net downward SW radiation indicative of too little cloud.

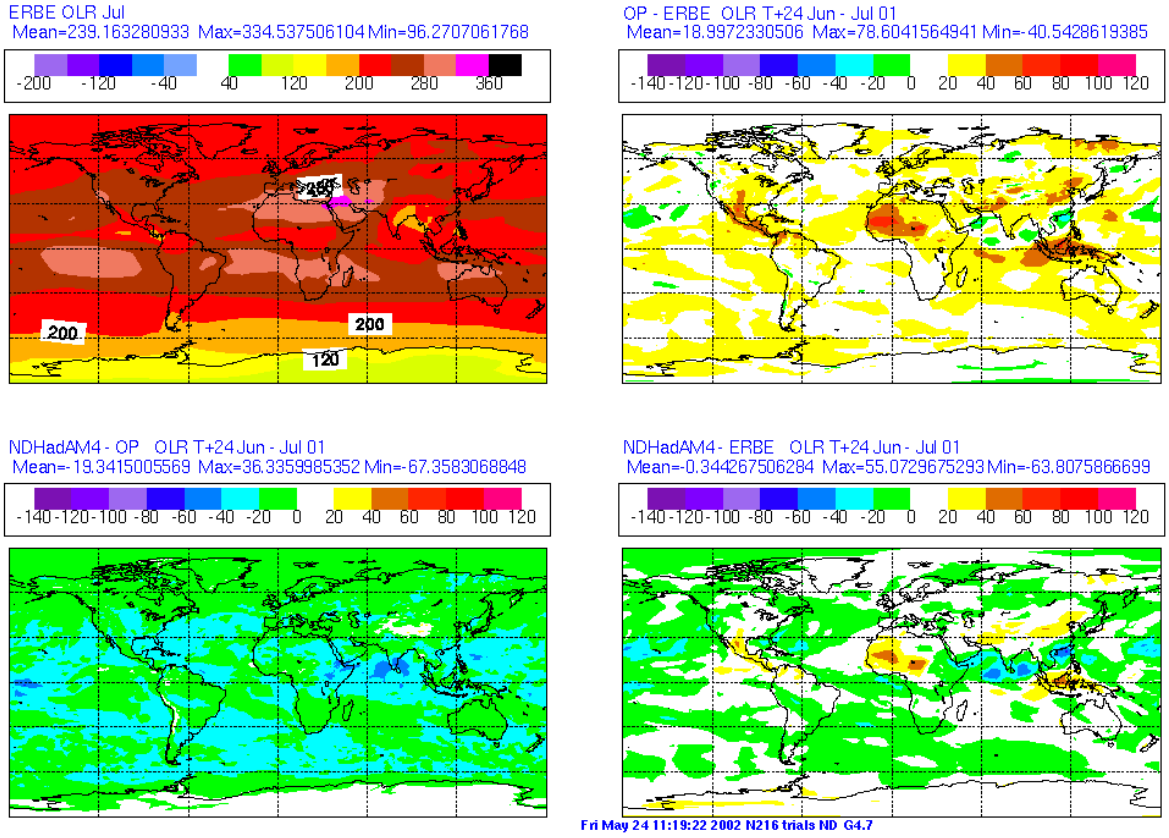

Figure 37 *- Outgoing longwave radiation (OLR) at top of the atmosphere (W/m^2). ERBE estimate for July (top left); G26 - ERBE for Jun-Jul 01 forecasts (top right); forecast difference G27 - G26 (bottom left); G27 - ERBE (bottom right).*

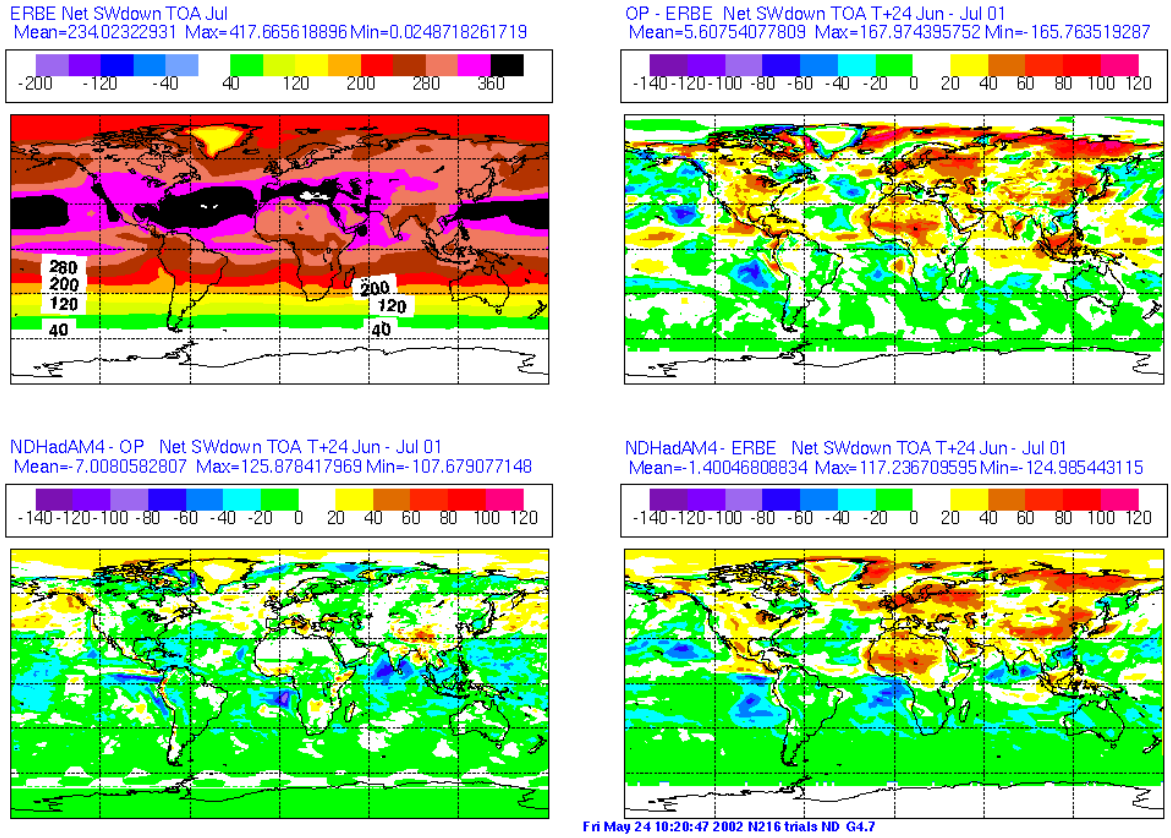

Figure 37: *as figure 37 but for net shortwave radiation*

Table 1 - Top of the atmosphere radiative fluxes for Jun-Jul 2001 forecasts of G27 and G26

	ERBE	G26	G27
OLR	239.16	258.2	238.8
Net downward SW	234.02	239.6	232.6

9. Summary

A brief summary of positive and negative points of tropical performance in cycle G27 of the global NWP model (New Dynamics and revised physics) is given below.

Advantages

- Improved prediction of tropical cyclones.
- Improved marine stratocumulus prediction.
- Improved top-of-the atmosphere radiation balance.
- Reduced stratospheric cold bias

Disadvantages

- Objective verification scores degraded - particularly at 250hPa and in Jun-Jul.
- Increased errors in the divergent circulation and associated errors in the rotational wind fields.
- Increased warm bias in the tropical mid-troposphere.
- G27 more susceptible to gridpoint storms.

Some indication from diagnostics is that the 4A convection scheme may be partly responsible for some of the increased diabatic heating and warm biases in the current versions of G27.

However, the change to the convective momentum transport closure with version 4A of the convection was clearly beneficial in reducing the errors in the 850hPa tropical winds.

The circulation errors in G26 and G27 are very similar, but errors in G27 tend to be almost twice the magnitude. It is unlikely that we can change the geographical distribution of these long-standing errors in the short-term, but the hope is we can impact on their magnitude. Further sensitivity of tests of tropical performance to the parametrizations in cycle G27 have been explored in an aquaplanet version of the Unified Model and these results are discussed in Milton et. al. (2003). Some promising results have been found in changing the diagnosis of the shallow convection scheme. In addition, a change was made to the operational model in December 2002 to include the MOSES 2 land surface exchange scheme (cycle G30 - see appendix). MOSES 2 seemed to increase the soil moisture availability in semi-arid regions, which in turn had positive impacts on tropical verification scores. These results will be discussed in detail in a forthcoming report. Ideas for further diagnostic work are outlined in the next section.

10. Ideas/questions for further work.

Further diagnostics

- A better definition of the hydrological cycle - spin up, P, P-E., cloud, fluxes, moisture (total column water and vertical variations)
- Land-sea split in diagnostics.
- Categorise errors/diagnostics by BL type?
- Time variation of tropical errors - hovmoller plots. More general investigation of tropical variability errors (may be best done in HadGEM tropical tiger team).
- How smooth is the diabatic forcing in space and time? - Look at timestep by timestep diagnostics.
- Improved diagnosis of cloud and radiative forcing - are the cloud distributions accurate? It may be best to deal with this in HadGEM1 where ISCCP diagnostics can be analysed
- Comparisons with HadGAM1/HadGEM1 - are we seeing the same errors in climate and NWP?

Numerical experiments (sensitivity tests)

- Convection - can we isolate the role of the momentum transports from the potential deficiencies in diabatic heating?
- Radiation - Can we further refine the spectral files based on more recent line-by-line data to improve tropical performance? Is the interaction with erroneous cloud (?) a barrier to any improvements?
- Boundary layer - what role is the BL turbulent mixing playing in determining the tropical circulation and cloud?
- What are the timestep sensitivities - both full timestep, convection and BL timestepping.
- Diffusion near steep orography? - Sensitivity of precipitation over tropical islands.
- Vertical diffusion - can this be replaced by a more intelligent stability based diffusion.

Idealised studies (see discussion paper by Woolnough, 2001)

- Aqua-planet at vn4.5 and vn5.2 - use this to investigate performance of parametrizations under idealised conditions.
- Dynamical core - what is the response of each dynamical core (vn5.2 and vn4.5) to idealised tropical heating profiles. Can we simulate the observed errors by imposing errors in heating functions in the dynamical core?
- Are there any comparisons with CRM that could help diagnose problems?

References

Cullen, M.J.P. and Davies, T.D, 1991: A conservative split-explicit integration scheme with fourth order horizontal advection. QJRMS, 117, 993-1002

Cullen, M.J.P., Davies, T, Mawson, M.H., James, J.A., Coulter, S., and Malcolm, A., 1997: An overview of numerical methods for the next generation UK NWP and climate model. In C.A. Lin, R.LaPrise, and H.Ritchie (editors), *Numerical methods in atmospheric and oceanic modelling, : The Andre Robert Memorial Volume*, pp 425-444.

Edwards, J.M., and Slingo, A., 1996: Studies with a flexible new radiation code I: Choosing a configuration for a large-scale model. QJRMS, 122, 689-719.

Esbensen, S., 1978: Bulk thermodynamic effects and properties of small tropical cumuli. JAS, 35, 826-837.

Huffman, G.J., R.F. Adler, P.Arkin, A.Chang, R.Ferraro, A. Gruber, J. Janowiak, B. Rudolf, U. Schneider, 1997: The global precipitation climatology project (GPCP) combined precipitation dataset. BAMS, 78, 5-20.

Fritsch, J.M., and C.F. Chappell, 1980: Numerical Prediction of Convectively Driven Mesoscale Pressure Systems. Part II. Mesoscale Model. JAS, 37, 1734-1762.

Gill, A.E., 1980: Some simple solutions for heat induced tropical circulation. QJRMS, 106,447-462.

Gregory, J.M., 1999: Representation of the radiative effect of convective anvils. Hadley Centre Technical Note 7.

Grant, A.L.M., and Brown, A.R., 1999: A similarity hypothesis for shallow cumulus transports. QJRMS, 125, 1913-1936.

Heming, J. and Greed, G., 2002: The Met Office 2002 global model upgrade and the expected impact on tropical cyclone forecasts. AMS 25th conference on hurricanes and tropical meteorology, (see http://ams.confex.com/ams/25HURR/25HURR/)

Jin, F and Hoskins, B.J., 1995:The direct response to tropical heating in a baroclinic atmosphere. JAS, 52, 307-319

Lock, A.P., Brown, A.R., Bush, M.R., Martin, G.M., and Smith, R.N.B., 2000: A new boundary layer mixing scheme. Part I: Scheme description and single column model tests. MWR, 128, 3177-3199

Matsuno, T., 1966: Quasi-geostrophic motions in the equatorial area. J. Met. Soc. Japan, 44, 25-43.

Milton, S.F., Willett, M., and Culverwell, I, 2003: Improving Tropical Performance: II Aquaplanet studies (to appear as Forecasting Research Technical Report).

Murphy, A.H., 1988: Skill scores based on the mean square error and their relationship to the correlation coefficient. MWR, 116,2417-2424.

Siebesma, A.P. and Cuijpers, J.W.M., 1995: Evaluation of parametric assumptions for shallow cumulus convection. JAS, 52, 650-666.

Simmons, A.J., Mureau, R. and Petroliagis, T., 1995: Error growth and estimates of predictability from the ECMWF forecasting system. QJRMS, 121, 1739-1771.

Staniforth, A., White, A., Wood, N., Thuburn, J., Zerroukat, M., and Cordero, E., 2002: The joy of U.M. 5.2 - Model Formulation. Unified Model Documentation paper No. 15 (Available from the Met Office).

Webster, S., Brown, A.R., Cameron, D.R., and Jones, C.P., 2002: Improvements to the representation of orography in the Met Office Unified Model. (Submitted to QJRMS).

Wheeler, M., and Kiladis, G.N., 1999: Convectively coupled equatorial waves: analysis of clouds and temperature in the wavenumber-frequency domain. JAS, 56, 374-399.

Wilson, C.A., 1992 : Vertical Diffusion. Unified Model Documentation Paper 21 - (Available from the Met Office).

Wilson, D.R. and Ballard, S.P., 1999: A microphysically based precipitation scheme for the U.K. Meteorological Office Unified Model. QJRMS, 125, 1607-1636.

Woolnough, S., 2001: Understanding the tropical performance of the UM: Idealised studies. (Discussion paper available from the author)

Appendix - Recent global model cycles.

CYCLE	Date	Description
G23	17 May 2000	MOSES I surface scheme implemented with weekly reset to climatology for soil moisture
G24	27 June 2000	Data assimilation upgrade • Use of scatterometer winds from ERS using variational dealiasing and quality control • Improved humidity error correlations • Increased use of AMSU-A radiances (ch 5) in cloudy areas • Introduction of surface wind speeds from a second (F15) SSM/I satellite • Introduction of wind profiler information
G25	18 Apr 2001	Data assimilation upgrade: • Stop using NOAA14 TOVS data • Start using NOAA16 ATOVS data • Also data from the AMSU-B instrument on NOAA15 and NOAA16.
G26	16 Oct 2001	Data assimilation upgrade: • Increase Observation errors for AMVs • Revise thinning of ATOVS to give preference to MW-clear over IR-clear • Use of fractional sea-ice in ATOVS processing
G27	**7 Aug 2002**	**Introduction of semi-implicit, semi-Lagrangian, non-hydrostatic dynamical formulation and revised physics package.**
G28	1 Oct 2002	Include NOAA-17
G29	4 Dec 2002	Change global data cut-off from 3h to 1h50m.
G30	11 Dec 2002	• Introduce Moses II land surface scheme • Introduction of Seawinds • Replacement of Meteosat SATOB winds with BUFR winds. • A correction to introduce time interpolation of pressure during pre-processing of observations in the OPS.